Astronomy & Astrophysics manuscript no. 0647 February 11, 2004
(DOI: will be inserted by hand later)

Identification of Emission Lines in the Low-Ionization Strontium Filament Near Eta Carinae⋆

H. Hartman[1], T. Gull[2], S. Johansson[1], N. Smith[3⋆⋆], and HST Eta Carinae Treasury Project Team ⋆⋆⋆

[1] Atomic Astrophysics, Lund Observatory, Lund University, Box 43, SE-221 00 Lund, Sweden
[2] Laboratory for Astronomy and Solar Physics, Code 681, Goddard Space Flight Center, Greenbelt, MD, USA, 20771
[3] CASA, 389 UCB, University of Colorado, Boulder, CO, 80309

Received ¡date¿ / Accepted ¡date¿

Abstract. We have obtained deep spectra from 1640 to 10100Å with the Space Telescope Imaging Spectrograph (STIS) of the Strontium Filament, a largely neutral emission nebulosity lying close to the very luminous star Eta Carinae and showing an uncommon spectrum. Over 600 emission lines, both permitted and forbidden, have been identified. The majority originates from neutral or singly-ionized iron group elements (Sc, Ti, V, Cr, Mn, Fe, Co, Ni). Sr is the only neutron capture element detected. The presence of Sr II, numerous strong Ti II and V II lines and the dominance of Fe I over Fe II are notable discoveries. While emission lines of hydrogen, helium, and nitrogen are associable with other spatial structures at other velocities within the Homunculus, no emission lines from these elements correspond to the spatial structure or velocity of the Sr Filament. Moreover, no identified Sr Filament emission line requires an ionization or excitation energy above approximately 8 eV. Ionized gas extends spatially along the aperture, oriented along the polar axis of the Homunculus, and in velocity around the Strontium Filament. We suggest that the Strontium Filament is shielded from ultraviolet radiation at energies above 8 eV, but is intensely irradiated by the central star at wavelengths longward of 1500Å.

Key words. Line: identification, circumstellar matter, Stars: kinematics, Stars: individual: Eta Carinae

1. Introduction

The Luminous Blue Variable star (LBV) Eta Carinae (η Car) experienced a major outburst in the 1840's with a secondary outburst in the 1890's (Davidson & Humphreys 1997, and references therein). Several solar masses of material were ejected, which is now directly seen as the expanding Homunculus (Morse et al. 1998; Smith et al. 2003b) and the Little Homunculus (Ishibashi et al. 2003). Although the central star provides 5x10^6 L$_\odot$ at a characteristic temperature of 25,000°K, most of the gas in the Homunculus is neutral (Davidson et al. 2001). The hollow bipolar lobes with an intervening equatorial skirt are seen primarily by dust-scattered radiation from η Car. STIS CCD spectra, recorded with a long aperture (52″ × 0.″2), revealed a thin, interior skin in the light of [Fe II] and [Ni II], but no H II nor He I, emission. Davidson et al. (2001) used these lines, and the absorption H and K lines of Ca II, to trace the inner, neutral surface of the Homunculus. Ground-based observations in the near-infrared (Smith 2002) revealed molecular hydrogen in the cool exterior of the Homunculus shell. Lines of Fe II, Hα and [Ni II] revealed an internal emission nebulosity, called the Little Homunculus (Gull & Ishibashi 2001; Ishibashi et al. 2003). Several bright, ionized emission structures exist very close to η Car, known as the Weigelt Blobs B, C and D (Weigelt & Ebersberger 1986), are located within 0.″1 to 0.″3 from the central star.

Damineli (1996) identified the 5.52-year period in the high-excitation nebular and stellar emission lines of η Car and its surrounding nebulosity. In a long-term monitoring series of programs to understand this variability, the Weigelt blobs B and D, along with η Car, have been observed with HST/STIS at nearly annual intervals since 1998 (Davidson et al. 1999; Gull et al. 2001). Over 2000 emission lines of the Weigelt blobs B and D were identified in the spectrum between 1700Å and 10300Å by Zethson (2001). Changes between the spectroscopic minimum in 1998 and the broad maximum during 1999 and 2000 demonstrate that lines of higher ionization disappear during the spectroscopic minimum only to reappear as the system recovers. Many H Lyα-pumped Fe II lines appear during the maximum (Johansson & Hamann 1993; Zethson 2001), and disappear during the minimum. The Fe II 2507, 2509 Å lines are the most enhanced of these fluorescence lines, and they feed

Send offprint requests to: Henrik Hartman, e-mail: henrik.hartman@astro.lu.se

⋆ Based on observations made with the NASA/ESA *Hubble Space Telescope*, obtained at the Space Telescope Science Institute, which is operated by the Association of Universities for Research in Astronomy, Inc., under NASA contract NAS5-26555.

⋆⋆ Hubble fellow

⋆⋆⋆ This research is partly based on data from the Eta Carinae Hubble Space Telescope Treasury project via grant no. GO-9420 from Space Telescope Science Institute.

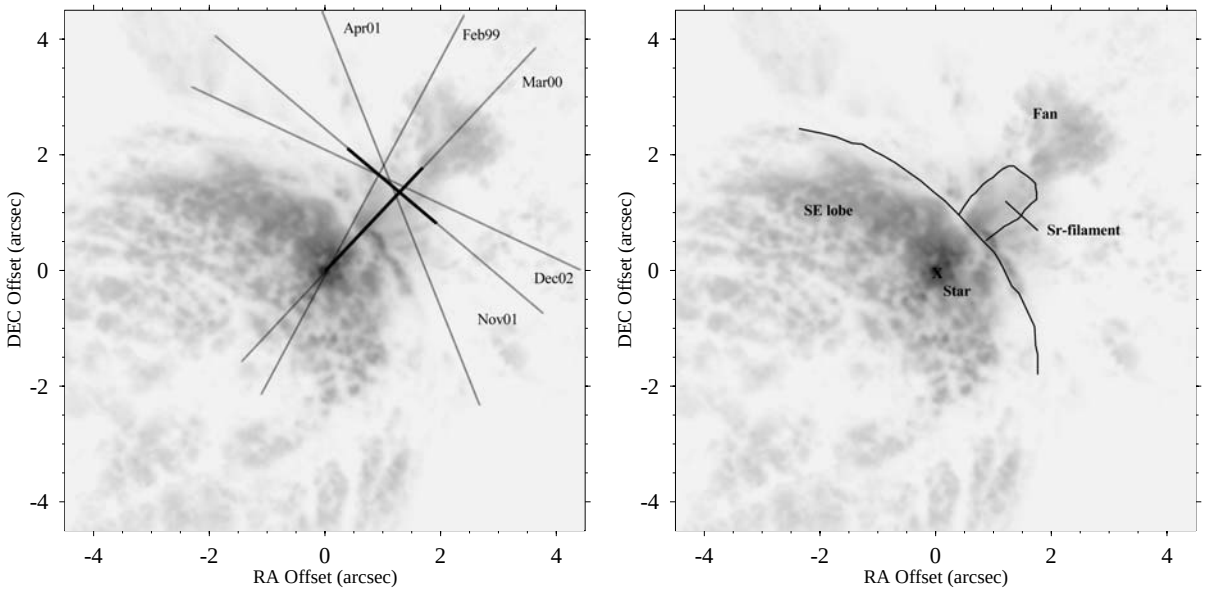

Fig. 1. ACS/HRC image of η Car and the Homunculus (Smith et al. 2004) with the aperture positions superimposed (See Table 1). The sections plotted in Fig. 2 and 3 are marked with bold lines. The March 2000 aperture represents the aperture centered on η Car. At this same epoch, multiple exposures were recorded with offsets orthogonal to the aperture to map the nebular structure (Ishibashi et al. 2003). We have used these same spectra to estimate the size of the Sr Filament in Sr II, sketched in the right panel.

long-lived Fe II states involved in a closed radiative cycle showing stimulated emission (Johansson & Letokhov 2003). Verner et al. (2002) used the CLOUDY model to predict the optical Fe II emission fluxes of the Weigelt B and D blobs during the spectroscopic minimum event of 1998.

During a preliminary test for the Homunculus mapping program in the 6400-7000 Å region planned as a STIS GTO Key Project (HST proposal 8483), we noticed some very faint, narrow emission lines located 1.5″ to the Northwest of η Car. The 1″ long emission filament appeared not to be associated with any known structure in η Car. Yet the spatial and velocity structure was similar for these lines and indicated that they must originate from the same volume. Zethson et al. (2001) identified twenty of twenty one lines in the 6400-7000A region, all originating from a structure moving at -100 km/sec. As the most spectacular discovery was the first identification of two [Sr II] lines, the filament became known as the Sr Filament. Peculiarly, no lines of hydrogen or helium were identified in the spectrum of this system. While lines of Fe II were not identified, lines of Fe I were. However, from the identifications of this wavelength limited spectrum it was not possible to conclude whether these emission lines were due to a selective excitation mechanism or to different elemental abundances.

The limited spectrum of the Sr Filament differed remarkably from similar spectra of other emission line nebular structures around η Car. This fact led to additional observations and line identifications in other wavelength regions. In the present paper we report on all HST observations obtained so far of the Sr Filament and tabulate all the measured emission lines. Nearly 600 lines have been identified, and only a few strong lines remain unidentified. We also discuss the peculiarities found in the spectrum in terms of apparent enhancements and depletions in elemental abundances, as well as clear indications of special ionization and excitation conditions in the filament.

2. Observations

The initial 6480 to 7000Å spectrum of the Sr Filament differed markedly from spectra of other emission line structures around η Car, and indeed from spectra of other nebulae. [Sr II] emission is not known to have been observed in other emission nebulae. Given the uniqueness of this nebular spectrum, we followed up with a series of observations, first to detect Sr II lines near 4000Å, then other nebular emission lines, within visits scheduled for η Car. Information on these visits are listed in Table I. The two resonance lines of Sr II at 4078 Å and 4216 Å were observed in emission. Bautista et al. (2002) found the Sr II line ratios to be consistent with a gas having electron densities of 10^7 cm^{-3} in a predominantly neutral region. We extended the spectral coverage across the entire range of the STIS CCD (1640 to 10100 Å), and examined the spectroscopic maps of the Homunculus in spectral intervals containing Hα and Hβ to determine the spatial extent of the peculiar emission. The observations were done during several HST visits. As the HST spacecraft orientation changes throughout the year, we had to accept observations through the long aperture at very different position angles (Figure 1). When possible, the aperture was centered on a common position offset 1.″5 at Position Angle 315° from η Car. Enough overlap in repeat spectral coverage (Table 1) allowed us to gain significant information on the spatial extent of the Sr Filament.

Direct imagery of the Sr Filament is not possible through the broad-bandpass filters available in the WFPC2 or the ACS cameras. The relatively weak emission lines are overwhelmed by dust-scattered starlight throughout the Homunculus. Other

Table 1. Log of Observations with the STIS

Date	HST Proposal	Offset from η Car R(″), θ	Pos Angle Degrees (N through E)	Aperture	Spectral Coverage Ångstroms
Feb 21, 1999	8036	0.4, 45°	-27.97°	52″ × 0.″1	6480-7000Å[1]
Mar 13, 2000	8327	0,0 [2]	-41.14°	52″ × 0.″2F2	2480-2910Å
					3795-4335Å
					4818-5100Å
					6480-7565Å[3,4]
					9300-9600Å
Mar 21, 2000	8483	$N \times 0.1$, 55°[5]	-35.02°	52″ × 0.″1	4818-5100Å
		$N \times 0.25$, 55°[5]			6480-7050Å
Apr 17, 2001	8619	1.″5, 315°	22.06°	52″ × 0.″2	4052-4593Å[6]
					4818-5100Å
					6480-7050Å[3]
Nov 27, 2001	8619	1.″5, 315°	-130.97°	52″ × 0.″2	2480-2633Å
					3022-10135Å[3,4,6]
Dec 16, 2002	9420	1.″5, 315°	-114.94°	52″ × 0.″2	1640-2492Å
					2897-3052Å

[1] Initial discovery spectrum (Zethson et al. 2001).
[2] Mar 13, 2000 observations were accomplished with the F2 (0.″85) fiducial blocking the η Car at the STIS entrance.
[3] Repeated spectra from 6480 - 7000Å to check for variability.
[4] Repeated spectra at 6995-7565Å to check variability
[5] Mapping spectra were recorded in the 4818-5100Å with 0.″1 offsets and 6480-7050Å spectral range with 0.″25 offsets to map the spatial structure of the Homunculus and the Little Homunculus. We used these spectra to estimate the size of the Strontium Filament in Fe II and [Sr II].
[6] Repeated spectra 4194-4593Å; 4818-5104Å to check variability

nebular emission structures with different photo-excitations, different spatial and velocity intervals are located in, or close to, the line of sight towards the Sr Filament. With direct imagery as in Figure 1 (Morse et al. 1998; Smith et al. 2004), we can trace the dusty structures of the Homunculus by the scattered, red starlight. Polarization measures using WFPC2 imagery (Schulte-Ladbeck et al. 1999; King et al. 2002) confirm the scattering properties of this light. The Little Homunculus was detected by multiple emission lines of Fe II, Cr II, etc in the near-ultraviolet, and may contribute to the ”purple haze”, associated with the feature commonly called the ’Fan’ within the Northwest lobe (Smith et al. 2004). Within the skirt, or the gas and dust structure located between the two lobes, bright emission lines extend over significant regions. Inspection of these emission lines indicate that some emission extends, in velocity and space, around the Sr Filament (Figure 2). The Sr Filament is best mapped with high spatial and moderate spectral resolution as produced by the STIS CCD moderate dispersion modes. Ground-based observations are currently limited to half-arcsecond seeing with much scattered light from the central star. The Sr Filament structure then becomes confused with other nebular emission and stellar emission.

Spectra of the Sr Filament were recorded through HST visits scheduled between February 1999 to December 2002 (2.8 years). This extends over the mid-portion of η Car’s broad spectroscopic maximum, which covers 5 years of the 5.52 year period. Highly excited emission lines of [Ne III], [Ar III] and He I, as monitored of the entire nebulosity by Damineli et al. (1998), changed slowly over this interval in nebular structure close to η Car (but these lines are not detected in the Sr Filament).

Given that these observations occur late in the broad spectroscopic maximum (when fluxes of all nebular lines appear to be relatively constant), we do not anticipate significant changes in the excitation of the Sr-Filament. The spectrum of the Weigelt Blobs, being at an order of magnitude closer to the Central Source, shows little change in the low-excitation emission lines of e.g. Fe II and Ni II across the entire 5.52-year cycle. Modeling by Verner et al (2002 and in preparation) demonstrates that the low-excitation emission lines are due largely to UV radiation longward of Lyman alpha. Most excitation of the Sr Filament appears to be due to mid-UV and near-UV, which changes little across the minimum. Smith et al. (2000) investigated the photometric variability in the ”purple haze” in WFPC2 pictures and found no evidence for variability that one might associate with the Sr filament, even during the 5.5 year cycle and the brightening of the star.

Where possible we repeated some spectral overlap to check for variability in emission line fluxes. The specific dates, HST programs, offsets from η Car, position angle, STIS aperture and spectral coverage are listed in Table 1. Locations of the aperture positions are overlaid on an Advanced Camera for Surveys (ACS) High Resolution Camera (HRC) ultraviolet image of the Homunculus (Smith et al. 2004) in Figure 1.

The discovery spectrum was recorded on February 21, 1999 under program 8036 (Zethson et al. 2001). Under program 8327, deep spectra were recorded on March 13, 2000 for two purposes: 1) we wanted deeper exposures of the Homunculus to infer the spatial structure of the lobes by the changes in velocity with position of locally-emitted narrow nebular emission lines and the locally-absorbed narrow absorption lines of Ca II

(Davidson et al. 2001), and 2) we wanted to extend the spectral coverage of the Sr Filament to other spectral regions as we anticipated that emission lines from additional elements in neutral and singly-ionized states would be detected. As most emission lines in the Homunculus are marginally resolved with the CCD G750M, G430M and G230MB gratings and the $52'' \times 0\farcs1$ aperture, a significant gain in limiting flux was obtained by using the $52'' \times 0\farcs2$ aperture. For this visit with STIS, we placed η Car behind the F2 fiducial ($0\farcs85$ wide), to prevent saturation of the CCD by the very bright star. On March 21, 2000 (program 8483), the Homunculus was mapped with the STIS using the $52'' \times 0\farcs1$ aperture and the grating settings for 6480-7000Å at $0\farcs25$ spacing and for 4818-5100Å at $0\farcs1$ spacing. The overall structure, with emphasis on the internal ionized regions called the Little Homunculus, is discussed by Ishibashi et al. (2003). We used these same data to map the Sr Filament. Deep spectra were recorded in April 2001 (program 8619) at wavelengths selected to obtain the fluxes of Sr II emission lines near 4100Å, to measure the width of the Sr Filament, and to detect additional emission lines. On November 27, 2001 (Program 8619), we recorded deep exposures from 3022-10135Å and 2480-2633Å as that was the region of the spectrum where many emission lines were predicted, including the Fe II lines at 2507Å and 2509Å. Based upon the non-detection of the Lyman-alpha-pumped Fe II lines at 2507 and 2509Å, we suspected that little or no hydrogen photo-ionizing radiation was impinging upon the Sr Filament. We expected that few emission lines would be detected below 2480Å. On December 16, 2002, we extended spectral coverage from 3052Å to 1640Å to gain full spectral coverage. No lines were detected shortward of 2489.7Å, which is an Fe I line of multiplet uv9. However, we caution the reader that the CCD sensitivity decreases rapidly below 2500Å. Deeper exposures would be possible with the MAMA detectors, likely in the E230M mode.

3. Kinematic structure of the strontium filament

The structure of the strontium filament is complex, and varies depending on the particular emission line observed. Since several distinct emission-line structures are seen projected along the same line of sight, the morphology needs to be understood before we can attempt to interpret the observed spectrum and assign line identifications. We know from previous study (Davidson et al. 2001; Smith 2002; Ishibashi et al. 2003) that at the position of the strontium filament there are at least three different structures: the equatorial skirt, the receding northwest polar lobe of the Homunculus (showing both intrinsic emission and reflected light), and the Little Homunculus. Fortunately, these different features can be disentangled by considering their Doppler shifts.

Figure 2 shows the kinematic structure at the position of the strontium filament. Two different position angles, perpendicular to one another, are chosen to sample its full spatial extent (see Figure 1). The resonance line Sr II λ4078 is the brightest of the four lines from Sr^+ that have been detected in our data (Zethson et al. 2001). [Ca II] is a much brighter line that traces gas in a similar ionization state; Ca^+ ranges from 6.1 to 11.9 eV, while Sr^+ has a range of 5.7 to 11.0 eV. Indeed, contours of [Ca II] superposed over Sr II emission show that both lines seem to trace the same gas.[1] The [Ca II] emission shows that the Sr filament is more than just a single thin "filament", and has a spatial extent of $\gtrsim 1\farcs5$ along the polar axis of the Homunculus, and $\gtrsim 2''$ in the direction perpendicular to the polar axis. Thus, the Sr Filament occupies the same spatial extent as the "purple haze" seen in *HST* images of η Car (Smith et al. 2004; Morse et al. 1998). The Sr Filament is constrained to heliocentric velocities between -50 and -300 km s^{-1}, and is probably in or near the equatorial plane. It appears to have two main velocity components; one at about -100 km s^{-1}, with a velocity structure tilted so that emission becomes more blueshifted with increasing separation from the star (in March 2000), and another feature at about -240 km s^{-1} with the opposite tilt. The -100 km s^{-1} component is brighter at most positions (at least in Sr II), and dominates the emission spectrum listed in Table 2. Interestingly, fainter extended emission in [Ca II] suggests that both these velocity components may be part of a single closed structure, forming a ring or loop in velocity space, especially in the November 2001 spectra.

Emission from [Ni II] λ7379, on the other hand, shows subtle differences compared to both Sr II and [Ca II]. It has two remarkably straight velocity components (top panel in Figure 2), both tilted in the same sense, both with blueshift increasing with separation from the star. Davidson et al. (2001) suggested that these two velocity components traced gas in the equatorial plane with two different ages, originating in the Great Eruption and the 1890 event (see Humphreys et al. 1999). Some of the [Ni II] emission coincides with Sr II and [Ca II], but some does not. In particular, the diffuse [Ni II] emission near position=$0''$ and -150 km s^{-1} in the bottom panel of Figure 2 seems to fill in the gap between the two velocity components of Sr II and [Ca II]. Perhaps this makes sense, since Ni^+ occupies ionization zones between 7.6 and 18.2 eV, only partly overlapping with Sr^+ and Ca^+. The velocity components of [Ni II] and [N II] at -40 km s^{-1} and redshifted velocities up to -300 km s^{-1} trace the northwest polar lobes of the Homunculus and Little Homunculus, respectively (Ishibashi et al. 2003; Smith et al. 2004). [N II] emission is *only* seen in these polar features, and is absent in the equatorial material, while [Ni II] is seen in both. These polar structures must be exposed to radiation above 12 eV, since Sr II and [Ca II] are absent. This reinforces the idea that the strontium filament is somehow shielded from radiation above 12 eV (even though the ionization potential of N is 14.5 eV, it can be ionized from the excited ^{2}D state by photons at $\sim$12.1 eV).

As noted above, the blueshifted velocities imply that the strontium filament may reside in or near the equatorial plane — this may be an important factor for understanding its unusual excitation. On the one hand, various clues suggest that η Car has an asymmetric radiation field, with more UV radiation escaping the stellar wind at low latitudes near the equator where the wind is thinner (Smith et al. 2003a, 2004), at least during its "normal" high-excitation state between spectro-

[1] In regions exposed to radiation above 11 to 12 eV, Sr and Ca will both be doubly ionized and difficult to detect because of their atomic structure.

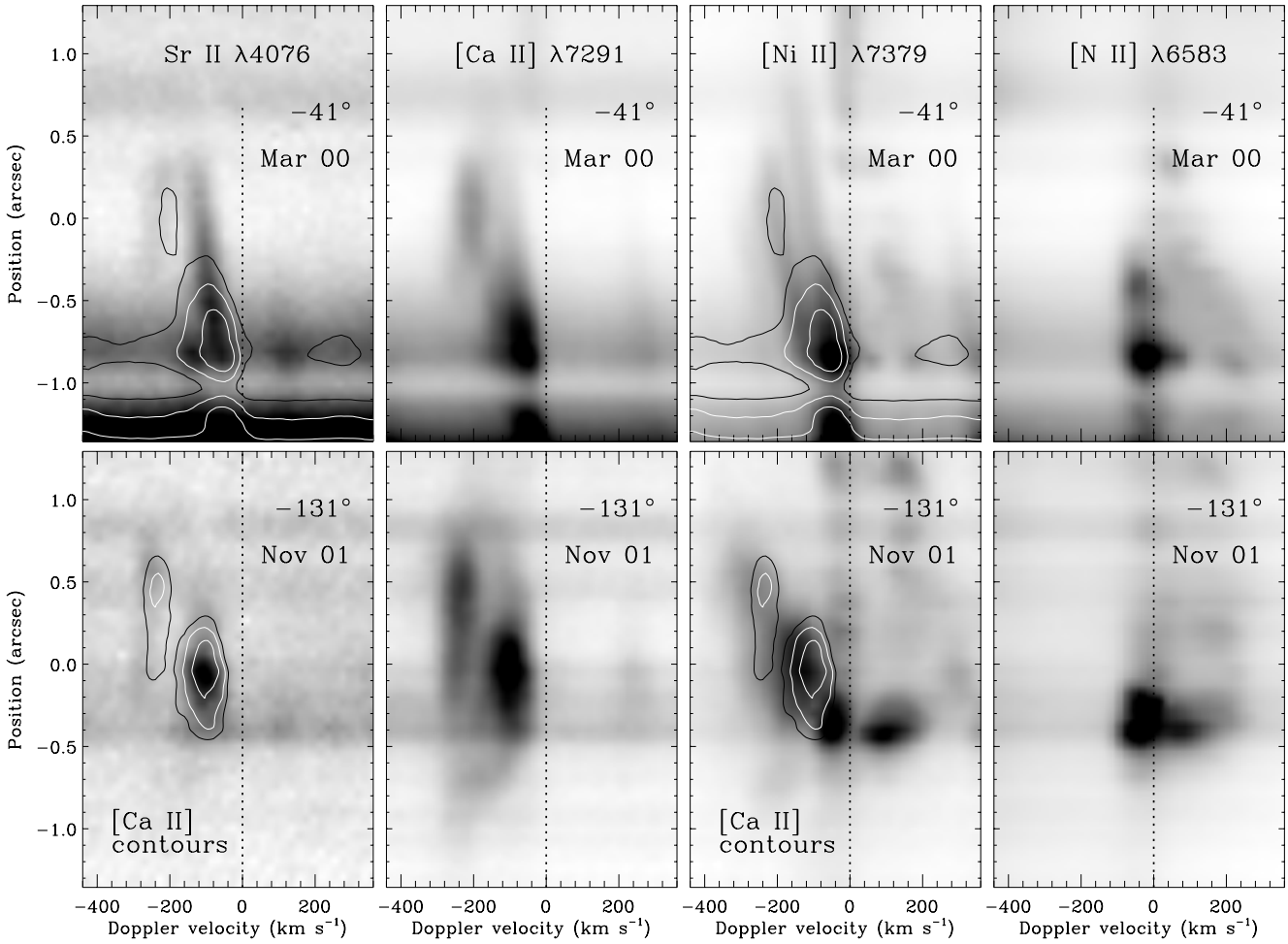

Fig. 2. Position-velocity diagrams at the location of the strontium filament seen in several different emission lines, with two different slit orientations. The top row shows spectra taken in March 2000 with the STIS slit at P.A.=-41°, and the bottom row shows the same four emission lines obtained in November 2001, with the slit at P.A.= −131° (see Figure 1 and Table 1). The four emission lines shown here are (left to right in both the top and bottom panels): Sr II λ4078, [Ca II] λ7293 (this is actually the average of [Ca II] λ7293 and [Ca II] λ7325), [Ni II] λ7379, and [N II] λ6585. The contours superposed on the Sr II and [Ni II] emission are corresponding contours of the [Ca II] emission at the same dates and slit positions. The horizontal axis shows heliocentric Doppler velocity. In the top and bottom panels, the position marked as zero corresponds roughly to the place where the two slits cross to within about 0.″1 (see Figure 1).

scopic events. On the other hand, there may be a considerable column of material between the star and the strontium filament, including the Weigelt objects and a larger-scale disk or torus, which may absorb all ionizing photons along that path but apparently transmits photons below 12 eV. In any case, both the strontium filament and the Weigelt objects appear to occupy a special azimuthal direction relative to η Car. In general, the subtle variations in emission structure from one tracer to the next suggest that the strontium filament is a low-ionization region with stratified ionization zones. This will be relevant in future efforts to model the emission spectrum (Bautista et al., in preparation).

During the April 2001 observation, the slit was oriented in a way that a region NE of the filament (i.e. ∼2” north of the star) was observed. This spatial region close to the filament shows a weak scattered continuum. In this continuum can be seen absorption lines from the allowed Sr II lines λ4078,4216 and the Ca I λ4227 line. For this slit orientation, there are only a few wavelength regions observed, but this absorption is not observed in any other lines. For all of the transitions showing this absorption, the lower level is the ground state, which might indicate that this is a low excitation region.

4. Line Identification

The spectra of the Sr Filament were observed at five different dates with a long aperture at different position angles as mentioned in Sec. 2 (See Figure 1 and Table 1). By inspection of individual visits, we know that there are very significant spatial variations of the nebular emission. Given the interval in time between all observations, there is the possibility of temporal variations. Other than in the region of close

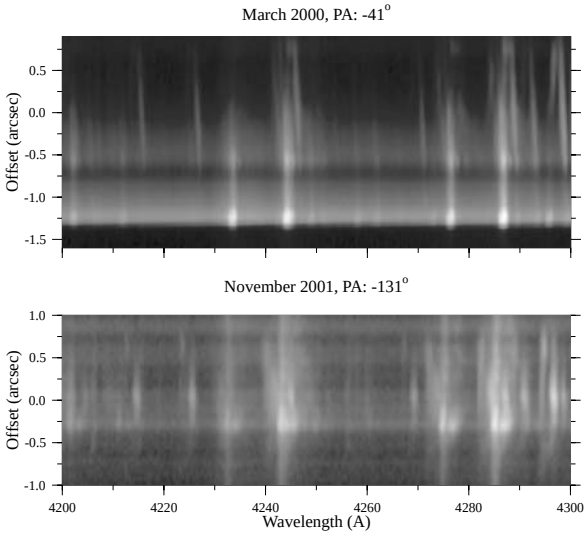

Fig. 3. 2D spectrum of the filament at two different slit orientations at nearly orthogonal angles, March 2000 and November 2001, respectively. The vertical stretch in the upper panel is 2.″5 and in the lower 2”. The horizontal scale covers the region 4200-4300Å. The aperture width was 0.”2 on the sky. The slit positions are shown projected on the Homunculus in Fig. 1 with the plotted regions marked with bold lines.

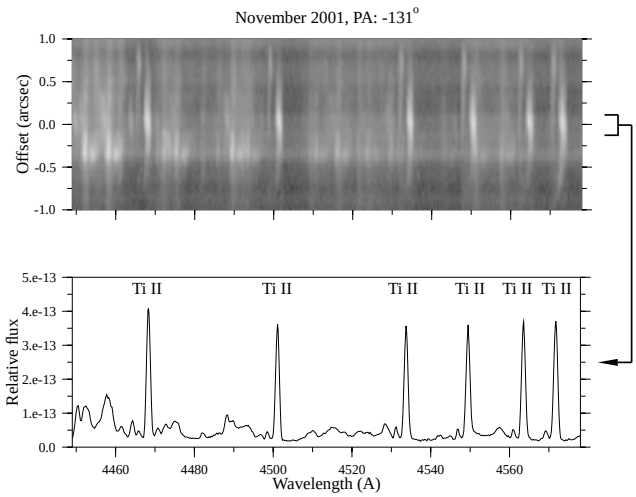

Fig. 4. Upper panel: Subsection of STIS nebular spectrum centered upon the Sr Filament . The STIS $52 \times 0.''2$ aperture was used for this spectrum. Lower panel: Extracted spectrum of the $0.''2 \times 0.''2$ area, marked on the right hand side of the nebular spectrum in the upper panel. This represents the central position of the Sr Filament.

overlap, there is also the strong possibility of spatial and/or temporal variations complicating the application of line ratios, especially if the relevant spectral lines were not measured in the same visit. However, some spectral regions were observed on several occasions. The different profiles for the same spectral line in different visits can then be compared. We also note that the bulk of the observations were taken thirteen months apart (in November 2001 and December 2002) at position angles within 16° of each other. The star is in the broad, high-excitation phase; temporal variability should be minimum across this time-span. Spatial variations appear to be small in the central core of the Sr Filament.

Some observed emission lines are likely the composite of emission from a number of regions along line of sight. The imaging properties of STIS along the aperture and the radial velocity shifts in the spectral direction enable us to disentangle the nebular emission for several kinematically different systems, as discussed in Sec. 3 above and seen in Fig. 2. Lines belonging to the filament show a Doppler shift of about -100 km/s at the center of the filament.

Examples of the spatial and velocity variations for two different slit orientations are presented in Figure 3. The aperture position angle was at $-41°$ (North through East convention) in March 2000 (upper plot) and is located in the general direction from η Car along the polar axis of the Homunculus. In the 2.″5 slice (top, Figure 3), the Sr Filament is centered at 0″. A velocity shift is noticeable in the spectral dispersion to the blue at 0.″5. The November 2001 observations was with the aperture positioned at $-131°$, or perpendicular to the Homunculus polar axis. The peak of the Sr Filament emission is positioned at 0″. There is little velocity shift along the slice of nebular in this direction. In Figure 4, a second slice of spectrum is shown for the November 2001 set of spectra (top). The extracted spectrum for a 0.″2-high extraction is plotted below. Note that all six bright lines are Ti II emission lines of the -100km/s Sr Filament. A much fainter second filament can be seen to the blue in both the spectral image (top) and the extracted spectrum(bottom). These two structures are plotted in velocity in Figure 2.

4.1. Linelist and intensities

All lines attributed to the Sr Filament are presented in Table 2. The major selection criteria are the shape of the line and its spatial location in the long-slit STIS spectrum (see Sec. 3). We do not observe any lines attributable to the Sr Filament in the region below 2480 Å. Little emission is observed below 2000 Å. Strong absorption along the line of sight from singly-ionized iron-group elements removes much light at these wavelengths, and the CCD sensitivity also declines in the mid-UV region. The absence of lines could also be linked to the possible presence of a lower wavelength limit for radiation available for ionization and excitation. Some faint emission lines are present but they may not be associable with the Sr Filament as emission lines are present from other regions along line of sight. The region 2500–3000 Å is less affected by absorption and shows emission lines. The region longward of 3000 Å contains well-defined Sr Filament emission lines, although emission from other spatial regions affects the spectrum.

The observed lines in Table 2 were measured in vacuo with heliocentric velocity corrections (column 1) and, where identified, include laboratory wavelengths (column 3). The difference between the two is converted to a velocity (km/s, column 2). The velocities are derived from the nov01 spectrum except for a few cases, when the mar00 (2630-3025 Å) spectra are used. The spectra include emission lines from other nebular

structures in line of sight, but only the lines associated with the strontium filament are included in the linelist. Some lines have measured velocities deviating from –100 km/s as they are either affected by absorption or blended by other lines. Blended lines, or lines with possible multiple identifications, are listed more than once with the identified wavelength, but with alternate wavelengths corresponding to the alternate line identifications. These lines are associated with the strontium filament despite the deviant Doppler velocity. The lines are identified by the species (e.g. Fe I), multiplet number and transition in columns 4-6. The transition is represented by the lower and upper level, using the *LS* term notation in Moore's tables of multiplets and energy levels. Thus, the term notation is preceded by a small letter a,b,c,etc. for even parity configurations and z,y,x,etc. for odd-parity configurations. If the multiplet is missing in Moore's tables we have inserted an abbreviated configuration notation. For full spectroscopic notations the reader is referred to the original laboratory line lists or to detailed atomic databases [2]. Intensities from the different STIS spectra are given in columns 7-10. Unidentified lines are marked with "unid" in the fourth column.

In Table 3 we have sorted the identified lines from Table 2 according to element, starting with the lightest element, carbon, and ending with the heaviest, strontium. Within each species the lines have been grouped after the excitation potential of the upper level, from which the line originates. The velocity for each line has been included to facilitate the study of consistency within each group of lines for a specific species.

4.2. Observed lines

The spectrum of the Sr Filament is dominated by permitted and forbidden lines of the iron group elements, as can be seen in Table 3. The spectrum is quite different from spectra of the Weigelt blobs (Zethson 2001) as regards the line and intensity distributions among the different elements. For example, lines of Fe I, V II and Ti II are particularly strong in the Sr Filament, whereas only a few Fe II lines are observed. Among the observed spectra are C I, Mg I, Al II, Ca I, Ca II, Sc II, Cr II, Mn II, Fe II, Co II, Ni II and Sr II. By contrast, lines of Fe II are dominant in the Weigelt blobs. Fe III and Fe IV lines are identified, but very few Fe I lines (Zethson 2001).

The spectral distribution of lines from a specific atom(ion) is determined by the atomic structure and the value of the ionization potential. Hence, the number of lines identified for different species reflects not only the abundance but also the complexity of the atomic structure. Assuming an upper limit of about 8 eV of the photon energy available for ionization and excitation (see Sec. 2) the number of observable emission lines from some spectra will be very small. We can divide the spectra of the observed species in three groups, corresponding to their atomic structure and referring to the periodic table:

I) Group 1A and 2A (Na I, Mg I, Al II, Ca I, Ca II, Sr II)
II) Group 3A-7A (C I)
III) 3d-elements (Sc - Ni)

Group I has quite simple spectra and the resonance lines appear in the optical region for the alkali atoms. In alkali spectra there are no forbidden spectral lines to observe, but the alkaline earth-like ions Ca I and Sr II show forbidden 3d-4s (4d-5s) transitions due to the similar binding energy of d- and s-electrons in transition group elements. In practice, these elements could therefore be placed in group III, where the overlap of 3d- and 4s configurations is the characteristic signature. In general, the number of lines increases with the number of valence electrons, i.e. the atomic number, for the transition elements, but decreases towards the end of the period when the d-shell gets closed. We see in Table 3 that there is a large number of lines of Sc II, Ti II and V II compared to Cr II, Mn II and Fe II. This excess of lines for the first elements of the transition group could thus be an abundance effect. However, we have to keep in mind that the ionization energy, and therewith also the excitation energy for the resonance lines increase with atomic number for the iron-group. A limited photon energy for radiative excitation favors the lightest iron-group elements, and the wavelengths of the resonance lines is below 2480 Å for the heavier ones.

Some single line identifications in Table 2 (and 3) are questionable either because the associated velocity differs remarkably from other lines or because the excitation energy is much higher than for other lines of the same species. However, the presence of the element is clear. As discussed above the presence of elements having a simple atomic structure is difficult to verify from the number of spectral lines. For example, aluminum is detected only by the inter-combination line of Al II and cannot be verified by other lines in the observed wavelength region, assuming similar excitation energies as for other elements. For comparison, we show in Figure 5 the situation for two spectra, Ti II and Sr II, where all allowed transitions within the observed wavelength range are included. The Einstein A-value (times the statistical weight of the upper level) is given on the horizontal axis as a measure of the line strength and the excitation energy of the upper level of the transition on the vertical axis. Among all possible transitions (marked with grey dots) the observed lines are marked with black dots. An expected trend of decreasing level population with increasing excitation energy can be seen. In addition, we also clearly see the larger number of predicted lines for Ti II due to a more complex atomic structure (Ti II has three and Sr II one electron outside closed shells).

No lines from hydrogen or helium that can be associated with emission from the Sr Filament have been detected. Neither have lines from nitrogen or oxygen. However, the spectrum includes the dust-scattered hydrogen Balmer P-Cygni stellar emission and could mask very weak nebular Balmer emission lines. The only neutron-capture element identified is strontium, but two of the unidentified lines, discussed in the next subsection, coincide in wavelength with Y II. However, they cannot be confirmed by other Y II lines having about the same probability to occur. Two of the unidentified lines coincide with the two strongest lines of the resonance multiplet of Zr II, a^4F-z^4G. Other than a coincidence with one other weak line, no other lines from Zr II are observed.

[2] e.g. http://physics.nist.gov/cgi-bin/AtData/main_asd at NIST or the data by Kurucz at http://cfa-www.harvard.edu/amdata/ampdata/kurucz23/sekur.html

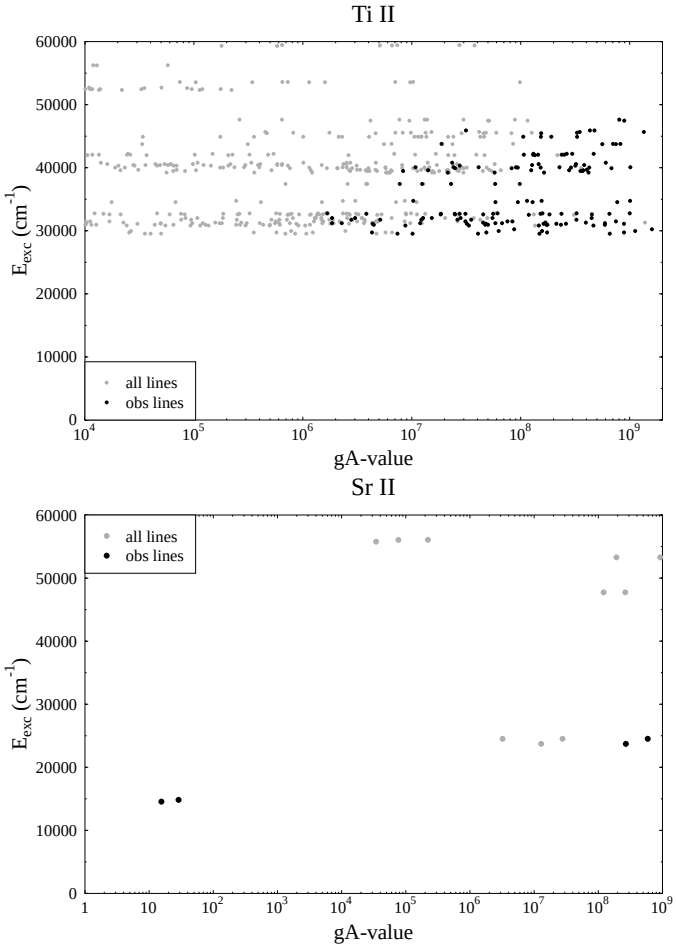

Fig. 5. Lines from Ti II (upper panel) and Sr II (lower panel) in the region 3000-10000 Å for Ti II and 3000-11000 Å for Sr II. All possible lines are shown in grey and the lines observed in the spectrum are in black. The difference in atomic structure is obvious. Note the different x-scales. The forbidden lines of [Ti II] are not included.

The line intensities from individual observations are included in Table 2. They are represented by the integrated flux in the emission feature, where contributions from obvious blending components have been subtracted. The tabulated flux is measured from intensity-calibrated spectra, which have not been corrected for interstellar reddening. Since the different observations do not cover the same spatial region the intensity ratios for different line pairs may not be the same in the different observations. In the wavelength regions affected by foreground absorption the intensity values are less reliable. Generally, the accuracy of the intensities is also affected by blending from other lines as well as from emission from the same line formed in other spatial regions along the line of sight. Some lines of e.g. [Fe II] and [Ni II] show complex profiles. The intensity contribution from the Sr Filament is difficult to determine. In such cases we used multi-Gaussian fits to extract the fluxes.

4.3. Unidentified lines

About 40 of the 600 observed lines in the spectra of the Sr Filament remain unidentified. These are marked with *unid* in Table 2 and listed in Table 4. A dozen unidentified lines have substantial strengths, as indicated in the intensity column of Table 4. For some of the lines we include possible identifications, but they should only be regarded as wavelength coincidences between observed lines and predicted transitions. The reasons for not including them among the identified lines could be a large Doppler velocity, an anomalous excitation energy or a general inconsistency with observed lines from the same ion.

Perhaps the most striking features of Table 4 are the wavelength coincidences of two Y II lines and of two Zr II lines and also the absence of candidates for identification of three of the strongest lines. The latter three lines appear below 2600 Å, which means that the corresponding photon energy is about 4.8 eV. This is remarkable, considering that 4.8 eV is not far from the highest excitation energy observed in the total spectrum and that all transitions between levels below 7-8 eV are known in ionized iron-group elements. The most probable explanation for these lines is that they originate from a neutral atom. However, as mentioned in section 4.1, this region suffers from absorption which can cause a shift in the observed wavelength and a significantly decreased measured line intensity. Emission from other spatial regions can also affect the lines.

5. Discussion

The Sr Filament proves to be a very unusual emission nebulosity. Over 600 emission lines, mostly from neutral and singly-ionized iron-peak elements, have been identified. Yet no hydrogen, helium, nitrogen or oxygen emission lines, which characterize normal emission regions, have been detected. Several factors contribute to this unlikely emission-nebula spectrum: 1) the very massive star system, while producing $5 \times 10^6 L_\odot$ with a characteristic temperature of $25,000\,^\circ K$ (Hillier et al. 2001), has a highly clumpy, extended but cool atmosphere (Verner et al. 2003); 2) much ionized gas shields this Sr Filament from hard UV radiation capable of ionizing hydrogen, and other elements requiring photo-ionizing energies exceeding 13.6eV; 3) apparently the shielding may be sufficient to protect the Sr Filament from radiation down to 6 or 7 eV as we see no direct evidence of line emission requiring photo-excitation with that energy; 4) an intense radiation field with energies less then 6 or 7 eV does bathe the Sr Filament, leading to a partially-ionized region; 5) the Sr II modelling (Bautista et al. 2002) indicates a very high-density region as the electron density must be in the range of 10^7 cm^{-3}.

We note that the ejecta surrounding η Car have a very non-uniform structure. While the overall Homunculus is a thin, hollow shell about ten percent thickness compared to the distance from the Central Source (Smith 2002; Smith et al. 2003b) the interior is likely a hot, low-density stellar wind. The thin surface interior to the shell is detected in [Fe II], [Ni II] emissions and Ca II absorption (Davidson et al. 2001; Smith 2002). In line of sight, ejecta absorptions of the iron-peak elements demonstrate a range of temperature and electron density that correlate with velocity (Gull, et al, ApJ submitted). Interior to the Homunculus is the Little Homunculus, a miniature bilobed structure (Ishibashi et al. 2003), which is seen in multiple emission lines of iron-peak elements and in the hy-

drogen Balmer lines. Between the bi-lobes of the Homunculus and the Little Homunculus is the skirt region, partially seen in emission lines, and in absorption lines. Close to η Car are several very intense emission knots, the Weigelt Blobs, seen strongly in many Fe II, Ni II, and Cr II lines (Zethson 2001). Highly-excited emission lines seen in the Weigelt Blobs and in the Little Homunculus disappeared during the 1998.0 and 2003.5 minima, but then returned. Low-excitation lines maintain constancy in flux throughout the 5.52-year period. As the Sr Filament emission lines are low-excitation only, this reinforces the concept that the Sr Filament receives radiation with the harder photons filtered out. Based upon the spatial distribution of the blue-shifted velocities, the Sr Filament is probably located in this equatorial skirt region. At a projected distance of the order of ten light-days, the Sr Filament receives intense mid-UV, and longer wavelength, radiation from the Central Source. Likely it is the strong absorption by iron and other iron-peak elements in the ionized regions and just beyond the ionized regions that shield the Sr Filament. We note that the ionization potential of Fe is 7.9 eV and that of Sr is 5.7 eV. As there is abundant Fe I and little Fe II in the Sr Filament, this indicates that the strontium is singly-ionized, but protected from becoming doubly-ionized by an iron-shield. Moreover, many Fe II absorptions are in the spectrum indicating the abundance of singly-ionized iron in the vicinity of the Sr Filament. Shortward of 2500Å, much of the ultraviolet spectrum is chopped up, further protecting the neutral and singly-ionized species with ionization potentials above 4 or 5 electron volts. Indeed the question arises as to whether molecular species might reside in this region. Ground-based, near-IR observations of the Homunculus (Smith 2002) do not indicate molecular hydrogen at these velocities or spatial position, but the ground-based observations were accomplished with lower spatial resolution.

We have systematically obtained spectra of the Sr Filament to characterize the spatial extent and the level of excitation through the identification of over 600 emission lines. We have also measured the fluxes of these lines in preparation for obtaining physical information of this neutral emission region. The first paper, based upon the Sr II emission line ratios, has been published, characterizing the temperature and density of the Sr Filament (Bautista et al. 2002), other papers will follow discussing models of other iron-peak neutral and singly-ionized species. We hope to provide information on relative abundances of various ionic species, possibly elemental abundances, but modelling and possibly some laboratory work will first be necessary.

Acknowledgements. We are grateful to Kazunori Ishibashi for providing calibrated spectra and giving inputs in the initial analysis. Other members of the HST Eta Carinae Treasury Project Team are Manuel Bautista, Michael Corcoran, Augusto Damineli, Kris Davidson (P.I.), Fred Hamann, John Hillier, Roberta Humphreys, Jon Morse, Otmar Stahl, Nolan Walborn and Kerstin Weis. This study is part of a project funded through a contract (S.J.) with the Swedish National Space Board. The data were obtained through the following HST observational programs: 8036, 8327, 8483, 8619 and 9420. Funding was provided under the STIS GTO program and HST GO programs. We acknowledge the assistance on the analysis by the STIS Instrument Definition Team (IDT), especially Don Lindler, Terry Beck and Keith Feggans. H.H. is grateful for travel support from the STIS IDT for a visit to Goddard Space Flight Center. N.S. was supported by NASA through grant HF-01166.01A from the Space Telescope Science Institute, which is operated by the Association of Universities for Research in Astronomy, Inc., under NASA contract NAS 5-26555. This research has made use of NASA's Astrophysics Data System Bibliographic Services.

References

Bautista, M. A., Gull, T. R., Ishibashi, K., Hartman, H., & Davidson, K. 2002, MNRAS, 331, 875

Damineli, A. 1996, ApJL, 460, L49

Damineli, A., Stahl, O., Kaufer, A., et al. 1998, A&AS, 133, 299

Davidson, K. & Humphreys, R. M. 1997, ARA&A, 35, 1

Davidson, K., Ishibashi, K., Gull, T. R., & Humphreys, R. M. 1999, in Eta Carinae at the Millennium, ASP Conf. Ser. 179. Edited by J.A. Morse, R.M. Humphreys, and A. Damineli., 227

Davidson, K., Smith, N., Gull, T. R., Ishibashi, K., & Hillier, D. J. 2001, AJ, 121, 1569

Gull, T. & Ishibashi, K. 2001, in Eta Carinae and Other Mysterious Stars: The Hidden Opportunities of Emission Spectroscopy, ASP Conf. Ser. 242. Edited by T.R. Gull, S. Johannson, and K. Davidson. San Francisco: Astronomical Society of the Pacific, 59

Gull, T., Ishibashi, K., Davidson, K., & Collins, N. 2001, in ASP Conf. Ser. 242: Eta Carinae and Other Mysterious Stars: The Hidden Opportunities of Emission Spectroscopy, 391

Hillier, D. J., Davidson, K., Ishibashi, K., & Gull, T. 2001, ApJ, 553, 837

Humphreys, R. M., Davidson, K., & Smith, N. 1999, PASP, 111, 1124

Ishibashi, K., Gull, T. R., Davidson, K., et al. 2003, AJ, 125, 3222

Johansson, S. & Hamann, F. 1993, Physica Scripta, T47, 157

Johansson, S. & Letokhov, V. S. 2003, Physical Review Letters, 90, 11101

King, N. L., Nota, A., Walsh, J. R., et al. 2002, ApJ, 581, 285

Moore, C. E. 1945, A multiplet table of astrophysical interest. (Princeton, N.J., The Observatory, 1945. Rev. ed.)

Morse, J. A., Davidson, K., Bally, J., et al. 1998, AJ, 116, 2443

Schulte-Ladbeck, R. E., Pasquali, A., Clampin, M., et al. 1999, AJ, 118, 1320

Smith, N. 2002, MNRAS, 337, 1252

Smith, N., Davidson, K., Gull, T. R., Ishibashi, K., & Hillier, D. J. 2003a, ApJ, 586, 432

Smith, N., Gehrz, R. D., Hinz, P. M., et al. 2003b, AJ, 125, 1458

Smith, N., Morse, J., & Gull, T.R., et al. 2004, ApJ, in press

Smith, N., Morse, J. A., Davidson, K., & Humphreys, R. M. 2000, AJ, 120, 920

Verner, E., Bruhweiler, F., Verner, D., Johansson, S., & Gull, T. 2003, ApJL, 592, L59

Verner, E. M., Gull, T. R., Bruhweiler, F., et al. 2002, ApJ, 581, 1154
Zethson, T. 2001, PhD thesis, Lund University
Zethson, T., Gull, T. R., Hartman, H., et al. 2001, AJ, 122, 322

Table 2. Spectral lines observed in the Sr-filament of η Car in the wavelength region 2480-10140 Å. The lines are sorted by wavelength.

λ_{obs} (Å)	Velocity (km/s)	λ_{lab} (Å)	Ion	Mult.	Transition[a]	I(mar00)	I(apr01)	I(nov01)	I(dec02)	Comment[b]
						(10^{-15} erg cm^{-2} s^{-1} arcsec^{-2})				
2489.71	-95	2490.501	FeI	(uv9)	a^5D_0-x^5F_1					
2490.61	-95	2491.395	FeI	(uv9)	a^5D_2-x^5F_3			20		
2491.05	-103	2491.907	FeI	(uv9)	a^5D_1-x^5F_2			4		
2492.53	-103	2493.383	FeI	(uv63)	a^5F_3-x^3G_3					
2492.82	-91	2493.573	FeI	(uv59)	a^5F_3-w^5G_2			22		
2510.71	-105	2511.591	FeI	(uv7)	a^5D_3-x^5D_2			45		
2537.92			unid					14		bl
2538.90			unid					22		
2540.88	-83	2541.585	ScII	(uv1)	a^3D_1-y^3P_2			8		
2540.88	-101	2541.735	FeI	(uv7)	a^5D_1-x^5D_2			8		
2545.08	-105	2545.967	ScII	(uv1)	a^3D_2-y^3P_2			8		
2548.76			unid					7		
2552.33	-93	2553.120	ScII	(uv1)	a^3D_3-y^3P_2			18		
2558.54	-288	2560.996	ScII	(uv1)	a^3D_2-y^3P_1			8		bl. abs
2563.16	-93	2563.958	ScII	(uv1)	a^3D_1-y^3P_0			24		
2566.69	-116	2567.682	FeII	(uv64)	$a^4D_{3/2}$-$z^4P_{1/2}$			15		
2576.00	-95	2576.820	FeI	(–)	a^3G_4-sp^3F_3			30		
2577.96	-86	2578.695	FeII	(uv78)	$a^4P_{1/2}$-$z^4P_{1/2}$			20		
2580.24			unid					37		
2590.73	-106	2591.646	FeI	(–)	a^5F_3-w^5P_2			11		
2592.96			unid					33		bl abs
2615-30		2607-2632	FeII	(uv1)	a^6D-z^6D					bl. abs
2663.42	-89	2664.214	CrII	(uv8)	$a^6D_{7/2}$-$z^6D_{9/2}$	20				
2663.42	-118	2664.467	CrII	(uv8)	$a^6D_{1/2}$-$z^6D_{1/2}$	20				
2665.93	-99	2666.813	CrII	(uv8)	$a^6D_{5/2}$-$z^6D_{7/2}$	10				
2669.07	-99	2669.949	AlII	(uv1)	$3s^2\ ^1S_0$-$3s3p\ ^3P^o_1$	17				
2672.62	-112	2673.621	CrII	(uv7)	$a^6D_{7/2}$-$z^4P_{5/2}$	13				
2677.07	-99	2677.955	CrII	(uv8)	$a^6D_{9/2}$-$z^6D_{9/2}$	21				
2677.07	-99	2677.957	CrII	(uv8)	$a^6D_{9/2}$-$z^6D_{9/2}$	21				
2678.53	-94	2679.371	VII	(uv3)	a^5D_3-z^5D_4	21				
2678.53	-118	2679.585	CrII	(uv8)	$a^6D_{3/2}$-$z^6D_{5/2}$	21				
2682.88	-88	2683.671	VII	(uv3)	a^5D_2-z^5D_2	5				
2682.88	-113	2683.887	VII	(uv3)	a^5D_0-z^5D_1	5				
2686.87	-113	2687.885	CrII	(uv8)	$a^6D_{5/2}$-$z^6D_{5/2}$	4				
2687.83	-104	2688.760	VII	(uv3)	a^5D_4-z^5D_4	5				
2688.73	-88	2689.519	VII	(uv3)	a^5D_4-z^5D_3	2				
2690.85	-82	2691.590	VII	(uv3)	a^5D_2-z^5D_1	10				
2690.85	-110	2691.839	CrII	(uv8)	$a^6D_{9/2}$-$z^6D_{7/2}$	10				
2698.46	-83	2699.210	CrII	(uv8)	$a^6D_{7/2}$-$z^6D_{5/2}$	11				bl.
2700.81	-103	2701.736	VII	(uv1)	a^5D_4-z^5F_5	11				
2701.99	-111	2702.989	VII	(uv2)	a^5D_3-z^3D_3	3				
2711.53	-103	2712.459	FeI	(uv47)	a^5F_4-w^5F_5	4				
2711.53	-112	2712.544	VII	(uv2)	a^5D_4-z^3D_3	4				
2713.53	-114	2714.564	TiII	(uv13)	$a^2D_{3/2}$-$y^2P_{3/2}$	7				
2714.35	-96	2715.218	FeII	(uv63)	$a^4D_{7/2}$-$z^4D_{5/2}$	13				
2715.63	-92	2716.463	VII	(uv1)	a^5D_2-z^5F_3	7				
2715.63	-102	2716.557	VII	(uv1)	a^5D_4-z^5F_4	7				
2719.04	-87	2719.833	FeI	(uv5)	a^5D_4-y^5P_3	10				
2720.85	-95	2721.709	FeI	(uv5)	a^5D_3-y^5P_2	6				
2727.59	-83	2728.347	FeII	(uv63)	$a^4D_{5/2}$-$z^4D_{3/2}$	28				
2730.77	-112	2731.790	FeI	(uv48)	a^5F_1-v^5D_1	22				
2733.52	-95	2734.390	FeI	(–)	a^5F_5-w^5D_4	7				
2736.92	-94	2737.776	FeII	(uv63)	$a^4D_{3/2}$-$z^4D_{1/2}$	15				

Table 2. Continued.

λ_{obs} (Å)	Velocity (km/s)	λ_{lab} (Å)	Ion	Mult.	Transition[a]	I(mar00)	I(apr01)	I(nov01)	I(dec02)	Comment[b]
						(10^{-15} erg cm^{-2} s^{-1} arcsec^{-2})				
2739.34	-112	2740.359	FeII	(uv63)	$a^4D_{7/2}$-$z^4D_{7/2}$	42				
2743.12	-97	2744.008	FeII	(uv62)	$a^4D_{1/2}$-$z^4F_{3/2}$	35				
2746.19	-121	2747.296	FeII	(uv62)	$a^4D_{1/2}$-$z^4F_{5/2}$					
2749.03	-120	2750.134	FeII	(uv62)	$a^4D_{5/2}$-$z^4F_{7/2}$	67				
2749.03	-138	2750.299	FeII	(uv63)	$a^4D_{1/2}$-$z^4D_{1/2}$	67				
2755.54	-110	2756.552	FeII	(uv62)	$a^4D_{7/2}$-$z^4F_{9/2}$	128				
2761.71	-100	2762.629	FeII	(uv63)	$a^4D_{1/2}$-$z^4D_{3/2}$	24				
2765.59	-98	2766.497	VII	(uv46)	a^3H_6-y^3G_5					
2810.23	-96	2811.134	TiII	(uv17)	$a^2P_{3/2}$-$y^2P_{3/2}$	8				
2813.39	-77	2814.116	FeI	(uv44)	a^5F_4-y^5G_5					
2815.20			unid			3				
2816.21	-104	2817.191	TiII	(uv17)	$a^2P_{3/2}$-$y^2P_{1/2}$	2				
2817.29	-111	2818.332	VII	(120)	a^3D_1-w^3D_1	2				
2832.10	-97	2833.015	TiII	(uv7)	$a^2F_{5/2}$-$y^2F_{5/2}$	5				
2835.60	-91	2836.463	CrII	(uv5)	$a^6D_{9/2}$-$z^6F_{11/2}$	13				
2843.25	-88	2844.085	CrII	(uv5)	$a^6D_{7/2}$-$z^6F_{9/2}$	22				
2849.71	-102	2850.675	CrII	(uv5)	$a^6D_{5/2}$-$z^6F_{7/2}$	7				
2852.06	-95	2852.964	MgI	(uv1)	$3s^2\ ^1S_0$-$3s3p\ ^1P^o_1$	35				bl. abs
2855.63	-92	2856.509	CrII	(uv5)	$a^6D_{3/2}$-$z^6F_{5/2}$	10				
2858.79	-101	2859.749	CrII	(uv5)	$a^6D_{9/2}$-$z^6F_{9/2}$	16				
2862.44	-102	2863.412	CrII	(uv5)	$a^6D_{7/2}$-$z^6F_{7/2}$	8				
2865.12	-86	2865.943	CrII	(uv5)	$a^6D_{5/2}$-$z^6F_{5/2}$	9				
2866.76	-86	2867.582	CrII	(uv5)	$a^6D_{3/2}$-$z^6F_{3/2}$	11				
2877.47	-85	2878.282	TiII	(uv14)	$a^2G_{7/2}$-$y^2G_{7/2}$	7				
2879.93	-97	2880.861	VII	(uv12)	a^5F_3-z^5D_3	12				
2882.49	-88	2883.339	VII	(uv12)	a^5F_2-z^5D_2	10				
2884.04	-96	2884.960	TiII	(uv14)	$a^2G_{9/2}$-$y^2G_{9/2}$	9				
2889.55	-95	2890.463	VII	(uv12)	a^5F_1-z^5D_0	11				
2891.44	-108	2892.483	VII	(uv12)	a^5F_2-z^5D_1	9				
2892.57	-74	2893.279	VII	(uv12)	a^5F_4-z^5D_4	16				
2892.57	-96	2893.493	VII	(uv12)	a^5F_2-z^5D_2	16				
2893.22	-97	2894.159	VII	(uv12)	a^5F_4-z^5D_3	9				
2896.17	-90	2897.040	VII	(uv11)	a^5F_2-z^3D_3	6				
2902.98	-97	2903.913	VII	(uv11)	a^5F_1-z^3D_2	7			11	
2906.34	-99	2907.290	VII	(uv11)	a^5F_3-z^3D_3	9			15	
2907.48	-86	2908.310	VII	(uv10)	a^5F_4-z^5F_5	9			13	
2908.71	-98	2909.660	VII	(uv12)	a^5F_5-z^5D_4				17	
2917.28	-95	2918.207	VII	(2)	a^5F_2-z^5F_1				7	
2920.21	-102	2921.209	VII	(uv11)	a^5F_3-z^3D_2				23	
2920.21	-104	2921.226	VII	(2)	a^5F_2-z^5F_3				23	
2923.93	-95	2924.862	VII	(2)	a^5F_5-z^5F_5				37	
2930.60	-107	2931.649	VII	(2)	a^5F_3-z^5F_3				11	
2932.10	-39	2932.480	VII	(–)	b^3D_2-x^3P_1				40	bl.
2932.10	-110	2933.179	VII	(–)	b^3D_3-x^3P_2				40	bl.
2932.10	-185	2933.913	MnII	(uv5)	a^5S_2-z^5P_1				40	bl.
2934.29	-98	2935.249	VII	(2)	a^5F_1-z^5F_2				10	
2939.00	-119	2940.168	MnII	(uv5)	a^5S_2-z^5P_2				53	bl.
2941.41	-96	2942.347	VII	(2)	a^5F_2-z^5F_2				20	
2944.50	-94	2945.422	VII	(2)	a^5F_4-z^5F_3				33	
2948.93	-115	2950.067	MnII	(uv5)	a^5S_2-z^5P_3				51	
2952.09	-84	2952.922	VII	(2)	a^5F_3-z^5F_2				26	
2957.48	-91	2958.374	VII	(uv11)	a^5F_2-z^3D_1				18	
2966.76	-102	2967.764	FeI	(10)	a^5D_4-y^5F_5				13	

Table 2. Continued.

λ_{obs} (Å)	Velocity (km/s)	λ_{lab} (Å)	Ion	Mult.	Transition[a]	I(mar00)	I(apr01)	I(nov01)	I(dec02)	Comment[b]
						(10^{-15} erg cm^{-2} s^{-1} arcsec^{-2})				
2968.46	-79	2969.241	VII	(28)	a^5P_3-y^5D_4				18	
2970.42	-97	2971.382	FeII	(2)	$a^4D_{3/2}$-$z^6F_{5/2}$				35	
2979.54	-69	2980.224	FeII	(2)	$a^4D_{1/2}$-$z^6F_{3/2}$				28	bl.
2994.41	-89	2995.300	FeI	(9)	a^5D_3-y^5D_2				8	
2995.96	-91	2996.863	VII	(27)	a^5P_1-z^5P_2				7	
2999.49	-90	3000.387	FeI	(30)	a^5F_5-x^5F_5				7	
3001.18	-90	3002.079	VII	(27)	a^5P_3-z^5P_3				16	
3008.18	-83	3009.017	FeI	(9)	a^5D_1-y^5D_0				5	
3008.18	-100	3009.188	TiII	(85)	$a^2H_{9/2}$-$z^2H_{11/2}$				5	
3009.55	-90	3010.446	FeI	(30)	a^5F_4-x^5F_4				3	
3013.07	-91	3013.985	VII	(28)	a^5P_1-y^5D_1				4	
3014.79	-90	3015.694	VII	(27)	a^5P_2-z^5P_1				11	
3016.89	-116	3018.063	TiII	(85)	$a^2H_{11/2}$-$z^2H_{11/2}$				32	
3019.07	-78	3019.862	FeI	(30)	a^5F_3-x^5F_3				2	
3020.72	-79	3021.519	FeI	(9)	a^5D_4-y^5D_4				17	
3020.72	-81	3021.542	VII	(28)	a^5P_2-y^5D_1				17	
3020.72	-122	3021.953	FeI	(9)	a^5D_3-y^5D_3				17	
3025.73	-99	3026.724	FeI	(9)	a^5D_0-y^5D_1			5	4	
3029.67	-94	3030.611	TiII	(85)	$a^2H_{9/2}$-$z^2H_{9/2}$			7	10	
3033.40	-91	3034.318	VII	(123)	b^3H_6-z^3I_7			10	8	
3033.40	-129	3034.702	VII	(34)	a^3G_5-z^3H_6			10	8	
3037.24	-102	3038.273	FeI	(9)	a^5D_1-y^5D_2			8	6	
3041.76	-86	3042.623	FeI	(30)	a^5F_3-x^5F_4			6	1	
3041.76	-176	3043.549	FeI	(30)	a^5F_2-x^5F_3			6	1	
3047.29	-29	3047.583	TiII	(47)	$a^4P_{3/2}$-$z^4P_{5/2}$			16	7	
3047.29	-118	3048.491	FeI	(9)	a^5D_2-y^5D_3			16	8	
3050.49			unid					8	4	
3053.37	-90	3054.279	VII	(34)	a^3G_4-z^3H_5			10		
3057.52	-12	3057.646	TiII	(47)	$a^4P_{1/2}$-$z^4P_{3/2}$			17		
3057.52	-80	3058.335	FeI	(28)	a^5F_5-x^5D_4			17		bl. HP
3057.52	-144	3058.990	TiII	(47)	$a^4P_{5/2}$-$z^4P_{5/2}$			17		
3058.99	-97	3059.975	FeI	(9)	a^5D_3-y^5D_4			1		
3066.36	-103	3067.404	TiII	(47)	$a^4P_{3/2}$-$z^4P_{1/2}$			23		
3066.36	-74	3067.119	TiII	(5)	$a^4F_{5/2}$-$z^4D_{5/2}$			23		
3066.36	-87	3067.245	TiII	(5)	$a^4F_{3/2}$-$z^4D_{3/2}$			23		
3071.77	-38	3072.153	TiII	(47)	$a^4P_{5/2}$-$z^4P_{3/2}$			16		
3071.77	-122	3073.015	TiII	(5)	$a^4F_{7/2}$-$z^4D_{7/2}$			16		
3074.94	-116	3076.123	TiII	(5)	$a^4F_{5/2}$-$z^4D_{3/2}$			14		
3078.18	-134	3079.551	TiII	(5)	$a^4F_{7/2}$-$z^4D_{5/2}$			13		
3087.56	-134	3088.934	TiII	(5)	$a^4F_{9/2}$-$z^4D_{7/2}$			19		
3089.27	-101	3090.306	TiII	(90)	$b^2G_{7/2}$-$x^2F_{5/2}$			12		
3092.88	-109	3094.003	VII	(1)	a^5F_5-z^5G_6			35		
3092.88	-115	3094.056	VII	(39)	b^3G_5-y^3G_5			35		
3097.08	-98	3098.095	TiII	(67)	$b^4P_{3/2}$-$z^4P_{5/2}$			10		
3100.93	-61	3101.565	FeI	(28)	a^5F_3-x^5D_3			15		
3100.93	-87	3101.834	VII	(39)	b^3G_3-y^3G_3			15		
3102.09	-107	3103.189	VII	(1)	a^5F_4-z^5G_5			12		
3103.74	-94	3104.712	TiII	(90)	$b^2G_{9/2}$-$x^2F_{7/2}$			11		
3105.08	-89	3105.996	TiII	(67)	$b^4P_{1/2}$-$z^4P_{3/2}$			6		
3106.22	-90	3107.147	TiII	(67)	$b^4P_{5/2}$-$z^4P_{5/2}$			18		
3110.51	-105	3111.597	TiII	(67)	$b^4P_{3/2}$-$z^4P_{3/2}$			24		
3110.51	-105	3111.597	VII	(1)	a^5F_3-z^5G_4			24		
3118.06	-117	3119.277	VII	(1)	a^5F_2-z^5G_3			35		

Table 2. Continued.

λ_{obs} (Å)	Velocity (km/s)	λ_{lab} (Å)	Ion	Mult.	Transition[a]	I(mar00)	I(apr01)	I(nov01)	I(dec02)	Comment[b]
						(10^{-15} erg cm^{-2} s^{-1} arcsec^{-2})				
3120.09	-113	3121.264	CrII	(5)	$a^4D_{3/2}$-$z^4F_{5/2}$			34		
3120.09	-62	3120.730	TiII	(67)	$b^4P_{5/2}$-$z^4P_{3/2}$			34		
3120.09	-187	3122.041	VII	(1)	a^5F_5-z^5G_5			34		
3124.94	-90	3125.879	CrII	(5)	$a^4D_{5/2}$-$z^4F_{7/2}$			58		
3124.94	-119	3126.182	VII	(1)	a^5F_1-z^5G_2			58		
3124.94	-209	3127.117	VII	(1)	a^5F_4-z^5G_4			58		
3130.19	-93	3131.164	VII	(1)	a^5F_3-z^5G_3			15		
3131.93	-99	3132.961	CrII	(5)	$a^4D_{7/2}$-$z^4F_{9/2}$			15		
3133.19	-101	3134.235	VII	(1)	a^5F_2-z^5G_2			19		
3136.40	-100	3137.439	VII	(122)	b^3H_5-y^3H_5			9		
3145.23	-96	3146.237	VII	(1)	a^5F_3-z^5G_2			10		
3145.23	-98	3146.262	VII	(1)	a^5F_5-z^5G_4			10		
3146.64			unid					5		
3151.97	-115	3153.172	TiII	(10)	$b^4F_{5/2}$-$z^4D_{5/2}$			11		
3154.09	-98	3155.118	TiII	(10)	$b^4F_{3/2}$-$z^4D_{3/2}$			12		
3155.47	-104	3156.562	TiII	(37)	$a^2G_{9/2}$-$y^4D_{7/2}$			15		
3161.34	-76	3162.136	TiII	(10)	$b^4F_{3/2}$-$z^4D_{1/2}$			9		
3161.34	-128	3162.689	TiII	(10)	$b^4F_{5/2}$-$z^4D_{3/2}$			9		
3162.21	-121	3163.488	TiII	(10)	$b^4F_{7/2}$-$z^4D_{5/2}$			42		
3168.30	-109	3169.449	TiII	(10)	$b^4F_{9/2}$-$z^4D_{7/2}$			30		
3187.69	-88	3188.624	VII	(8)	a^3F_2-z^3F_2			34		
3190.59	-95	3191.602	VII	(8)	a^3F_4-z^3F_4			26		
3190.59	-114	3191.802	TiII	(26)	$a^2D_{5/2}$-$y^2F_{7/2}$			26		
3202.35	-105	3203.463	TiII	(26)	$a^2D_{3/2}$-$y^2F_{5/2}$			27		
3208.63			unid					8		
3216.69	-107	3217.833	TiII	(36)	$a^2G_{7/2}$-$y^2F_{7/2}$			26		
3216.69	-122	3217.992	TiII	(2)	$a^4F_{7/2}$-$z^4F_{9/2}$			26		
3218.18	-94	3219.193	TiII	(84)	$a^2H_{9/2}$-$y^2G_{7/2}$			19		
3222.49	-119	3223.774	TiII	(2)	$a^4F_{5/2}$-$z^4F_{7/2}$			9		
3224.08	-102	3225.172	TiII	(84)	$a^2H_{11/2}$-$y^2G_{9/2}$			32		
3228.48	-98	3229.534	TiII	(24)	$a^2D_{3/2}$-$z^2P_{1/2}$			69		
3228.48	-153	3230.130	TiII	(2)	$a^4F_{3/2}$-$z^4F_{5/2}$			69		
3228.48	-175	3230.364	TiII	(36)	$a^2G_{9/2}$-$y^2F_{7/2}$			69		
3233.73	-90	3234.705	VII	(61)	a^3D_3-y^3F_4			12		bl.
3233.73	-109	3234.901	FeI	(158)	z^7D_4-e^7P_4			12		
3236.01	-97	3237.052	TiII	(23)	$a^2D_{3/2}$-$y^2D_{3/2}$			23		
3236.01	-139	3237.512	TiII	(2)	$a^4F_{7/2}$-$z^4F_{7/2}$			23		
3239.04	-87	3239.979	TiII	(2)	$a^4F_{5/2}$-$z^4F_{5/2}$			17		
3239.04	-144	3240.598	TiII	(23)	$a^2D_{5/2}$-$y^2D_{3/2}$			17		
3241.34	-148	3242.930	TiII	(66)	$b^4P_{3/2}$-$y^4D_{3/2}$			14		
3248.42	-104	3249.542	TiII	(66)	$b^4P_{5/2}$-$y^4D_{7/2}$			41		
3252.79	-98	3253.855	TiII	(2)	$a^4F_{7/2}$-$z^4F_{5/2}$			13		
3252.79	-100	3253.879	TiII	(23)	$a^2D_{5/2}$-$y^2D_{5/2}$			13		
3254.07	-103	3255.186	TiII	(2)	$a^4F_{9/2}$-$z^4F_{7/2}$			18		
3255.92	-83	3256.826	FeII	(1)	$a^4D_{7/2}$-$z^6D_{7/2}$			19		
3261.39	-105	3262.525	TiII	(89)	$b^2G_{9/2}$-$z^2H_{11/2}$			44		
3261.39	-107	3262.557	TiII	(66)	$b^4P_{3/2}$-$y^4D_{5/2}$			44		
3267.46	-108	3268.632	VII	(7)	a^3F_2-z^3G_3			17		
3271.52	-99	3272.598	TiII	(66)	$b^4P_{5/2}$-$y^4D_{5/2}$			61		
3271.52	-137	3273.016	TiII	(66)	$b^4P_{1/2}$-$y^4D_{3/2}$			61		
3276.31	-69	3277.061	VII	(7)	a^3F_4-z^3G_5			59		
3276.31	-129	3277.716	TiII	(45)	$a^4P_{5/2}$-$z^4S_{3/2}$			59		
3278.15	-99	3279.237	TiII	(66)	$b^4P_{3/2}$-$y^4D_{3/2}$			60		

Table 2. Continued.

λ_{obs} (Å)	Velocity (km/s)	λ_{lab} (Å)	Ion	Mult.	Transition[a]	I(mar00)	I(apr01)	I(nov01)	I(dec02)	Comment[b]
						(10^{-15} erg cm^{-2} s^{-1} arcsec^{-2})				
3278.15	-157	3279.868	TiII	(24)	$a^2D_{5/2}$-$z^2P_{3/2}$			60		
3282.06	-111	3283.271	TiII	(66)	$b^4P_{1/2}$-$y^4D_{1/2}$			55		
3287.72	-81	3288.608	TiII	(89)	$b^2G_{7/2}$-$z^2H_{9/2}$			47		
3287.72	-165	3289.531	TiII	(66)	$b^4P_{3/2}$-$y^4D_{1/2}$			47		
3295.98	-72	3296.766	FeII	(1)	$a^4D_{3/2}$-$z^6D_{3/2}$			14		
3298.60	-99	3299.684	VII	(7)	a^3F_4-z^3G_4			5		
3308.64	-101	3309.757	TiII	(7)	$b^4F_{7/2}$-$z^4F_{9/2}$			29		
3315.15	-102	3316.268	TiII	(65)	$b^4P_{1/2}$-$z^4S_{3/2}$			14		
3317.85	-102	3318.978	TiII	(7)	$b^4F_{5/2}$-$z^4F_{7/2}$			24		
3321.56	-99	3322.655	TiII	(65)	$b^4P_{3/2}$-$z^4S_{3/2}$			23		
3322.76	-103	3323.897	TiII	(7)	$b^4F_{9/2}$-$z^4F_{9/2}$			48		
3326.62	-101	3327.734	TiII	(7)	$b^4F_{3/2}$-$z^4F_{5/2}$			25		
3329.29	-101	3330.411	TiII	(7)	$b^4F_{7/2}$-$z^4F_{7/2}$			43		
3331.91	-105	3333.069	TiII	(65)	$b^4P_{5/2}$-$z^4S_{3/2}$			21		
3335.04	-101	3336.157	TiII	(7)	$b^4F_{5/2}$-$z^4F_{5/2}$			38		
3340.47	-77	3341.320	TiII	(7)	$b^4F_{3/2}$-$z^4F_{3/2}$			28		
3341.46	-124	3342.841	TiII	(16)	$a^2F_{5/2}$-$z^2G_{7/2}$			3		
3343.84	-80	3344.726	TiII	(7)	$b^4F_{9/2}$-$z^4F_{7/2}$			49		
3346.31	-125	3347.708	TiII	(7)	$b^4F_{7/2}$-$z^4F_{5/2}$			8		
3348.81	-107	3350.000	TiII	(16)	$a^2F_{7/2}$-$z^2G_{9/2}$			38		
3348.81	-90	3349.811	TiII	(7)	$b^4F_{5/2}$-$z^4F_{3/2}$			38		
3348.81	-140	3350.371	TiII	(1)	$a^4F_{9/2}$-$z^4G_{11/2}$			38		
3353.58	-99	3354.688	ScII	(12)	a^1D_2-z^1F_3			12		
3360.51	-150	3362.184	TiII	(1)	$a^4F_{7/2}$-$z^4G_{9/2}$			42		
3360.51	94	3359.456	CrII	(4)	$a^4D_{5/2}$-$z^6D_{3/2}$			42		bl.
3360.51	-12	3360.643	ScII	(4)	a^3D_2-z^3P_2			42		
3360.51	-154	3362.231	ScII	(4)	a^3D_1-z^3P_1			42		
3367.61	-125	3369.009	CrII	(3)	$a^4D_{7/2}$-$z^4P_{5/2}$			17		
3369.00	-80	3369.904	ScII	(4)	a^3D_2-z^3P_1			2		
3372.18	-83	3373.117	ScII	(4)	a^3D_3-z^3P_2			33		
3372.18	-89	3373.181	TiII	(16)	$a^2F_{7/2}$-$z^2G_{7/2}$			33		
3372.18	-141	3373.769	TiII	(1)	$a^4F_{5/2}$-$z^4G_{7/2}$			33		
3379.87			unid					19		
3379.87	-122	3381.250	TiII	(1)	$a^4F_{9/2}$-$z^4G_{9/2}$			19		
3383.14	-124	3384.541	TiII	(63)	$b^4P_{3/2}$-$y^2D_{5/2}$			15		
3383.14	-142	3384.740	TiII	(1)	$a^4F_{3/2}$-$z^4G_{5/2}$			15		
3387.64	-104	3388.819	TiII	(1)	$a^4F_{7/2}$-$z^4G_{7/2}$			29		
3391.76			unid					15		
3394.16	-123	3395.554	TiII	(63)	$b^4P_{5/2}$-$y^2D_{5/2}$			14		
3402.47	-82	3403.400	TiII	(54)	$a^2P_{1/2}$-$z^2P_{3/2}$			16		
3407.33	-212	3409.735	CrII	(4)	$a^4D_{7/2}$-$z^6D_{5/2}$			14		
3409.61	-105	3410.799	TiII	(1)	$a^4F_{7/2}$-$z^4G_{5/2}$			13		
3414.65			unid					7		
3416.15			unid					13		
3422.36	16	3422.183	CrII	(3)	$a^4D_{1/2}$-$z^4P_{1/2}$			25		
3422.36	-119	3423.714	CrII	(3)	$a^4D_{5/2}$-$z^4P_{3/2}$			25		
3438.51			unid					34		
3440.37	-107	3441.592	FeI	(6)	a^5D_4-z^5P_3			6		
3441.64	-116	3442.974	MnII	(3)	a^5D_4-z^5P_3			88		
3444.10	-105	3445.301	TiII	(6)	$b^4F_{9/2}$-$z^4G_{11/2}$			33		
3452.57	-78	3453.467	TiII	(99)	$b^2P_{1/2}$-$y^2P_{1/2}$			10		
3456.30	-94	3457.378	TiII	(99)	$b^2P_{3/2}$-$y^2P_{3/2}$			18		
3459.98	-115	3461.307	MnII	(3)	a^5D_3-z^5P_2			69		

Table 2. Continued.

λ_{obs} (Å)	Velocity (km/s)	λ_{lab} (Å)	Ion	Mult.	Transition[a]	I(mar00)	I(apr01)	I(nov01)	I(dec02)	Comment[b]
						(10^{-15} erg cm^{-2} s^{-1} arcsec^{-2})				
3461.30	-103	3462.486	TiII	(6)	$b^4F_{7/2}$-$z^4G_{9/2}$			8		
3465.65	-105	3466.853	FeI	(6)	a^5D_1-z^5P_1			6		
3473.77	-110	3475.035	MnII	(3)	a^5D_3-z^5P_3			71		
3473.77	-117	3475.124	MnII	(3)	a^5D_2-z^5P_1			71		
3477.04	-99	3478.183	TiII	(6)	$b^4F_{5/2}$-$z^4G_{7/2}$			44		
3482.53	-118	3483.902	MnII	(3)	a^5D_2-z^5P_2			64		
3488.33	-116	3489.675	MnII	(3)	a^5D_1-z^5P_1			44		
3490.87	-103	3492.065	TiII	(6)	$b^4F_{3/2}$-$z^4G_{5/2}$			42		
3496.29	-47	3496.833	MnII	(3)	a^5D_0-z^5P_1			65		
3496.29	-130	3497.810	MnII	(3)	a^5D_3-z^5P_3			65		
3504.63	-109	3505.899	TiII	(88)	$b^2G_{9/2}$-$y^2G_{9/2}$			43		
3510.71	-98	3511.849	TiII	(88)	$b^2G_{7/2}$-$y^2G_{7/2}$			23		
3517.14	-100	3518.307	VII	(6)	a^3F_4-z^5D_3			20		
3520.10	-100	3521.271	TiII	(98)	$b^2P_{1/2}$-$x^2D_{3/2}$			18		
3524.48	-106	3525.719	VII	(5)	a^3F_3-z^3D_3			8		
3530.60	-100	3531.769	VII	(4)	a^3F_2-z^5F_1			15		
3535.27	-98	3536.420	TiII	(98)	$b^2P_{3/2}$-$x^2D_{5/2}$			17		
3535.27	-123	3536.725	ScII	(11)	a^1D_2-z^1P_1			17		
3545.08	-95	3546.206	VII	(5)	a^3F_3-z^3D_2			18		
3556.67	-97	3557.811	VII	(5)	a^3F_4-z^3D_3			25		
3558.28	-107	3559.548	ScII	(3)	a^3D_2-z^3D_3			9		
3565.58	-69	3566.397	FeI	(24)	a^5F_3-z^3G_4			2		
3565.58	-118	3566.986	TiII	(40)	$a^4P_{3/2}$-$z^2S_{1/2}$			2		
3567.64	-90	3568.715	ScII	(3)	a^3D_1-z^3D_2			11		
3569.98	-95	3571.116	FeI	(24)	a^5F_4-z^3G_5			14		
3572.34	-101	3573.546	ScII	(3)	a^3D_3-z^3D_3			8		bl. HP
3576.25	-93	3577.361	ScII	(3)	a^3D_2-z^3D_2			24		
3580.93	-86	3581.947	ScII	(3)	a^3D_1-z^3D_1			25		
3580.93	-108	3582.217	FeI	(23)	a^5F_5-z^5G_6			25		
3584.99	-114	3586.342	FeI	(23)	a^5F_3-z^5G_3			9		
3587.15	-72	3588.008	FeI	(23)	a^5F_2-z^5G_2			14		
3589.75	-76	3590.656	ScII	(3)	a^3D_2-z^3D_1			43		
3589.75	-85	3590.773	VII	(5)	a^3F_2-z^3D_1			43		
3589.75	-146	3591.499	ScII	(3)	a^3D_3-z^3D_2			43		
3591.91	-95	3593.050	VII	(4)	a^3F_3-z^5F_2			28		
3593.26	-92	3594.355	VII	(4)	a^3F_4-z^5F_3			23		
3595.90	-99	3597.078	TiII	(15)	$a^2F_{7/2}$-$z^4D_{5/2}$			19		
3600.62			unid					5		
3608.76	-94	3609.888	FeI	(23)	a^5F_1-z^5G_2			11		
3613.64	-101	3614.860	ScII	(2)	a^3D_3-z^3F_4			26		
3618.71	-90	3619.800	FeI	(23)	a^5F_2-z^5G_3			14		
3624.71	-95	3625.858	TiII	(52)	$a^2P_{1/2}$-$z^2S_{1/2}$			12		
3630.72	-87	3631.777	ScII	(2)	a^3D_2-z^3F_3			30		
3630.72	-147	3632.498	FeI	(23)	a^5F_3-z^5G_4			30		
3641.16	-100	3642.369	TiII	(52)	$a^2P_{3/2}$-$z^2S_{1/2}$			18		
3642.67	-95	3643.822	ScII	(2)	a^3D_1-z^3F_2			22		
3645.27	-89	3646.350	ScII	(2)	a^3D_3-z^3F_3			16		
3647.75	-93	3648.881	FeI	(23)	a^5F_4-z^5G_5			9		
3651.68	-95	3652.835	ScII	(2)	a^3D_2-z^3F_2			14		
3659.68	-92	3660.804	TiII	(75)	$b^2D_{5/2}$-$y^2F_{7/2}$			14		
3662.06	-100	3663.281	TiII	(75)	$b^2D_{3/2}$-$y^2F_{5/2}$			21		
3679.72	-101	3680.961	FeI	(5)	a^5D_4-z^5F_4			7		
3683.04	-87	3684.104	FeI	(5)	a^5D_3-z^5F_2			9		

Table 2. Continued.

λ_{obs} (Å)	Velocity (km/s)	λ_{lab} (Å)	Ion	Mult.	Transition[a]	I(mar00)	I(apr01)	I(nov01)	I(dec02)	Comment[b]
						(10^{-15} erg cm^{-2} s^{-1} arcsec^{-2})				
3684.99	-102	3686.238	TiII	(14)	$a^2F_{5/2}$-$z^2D_{3/2}$			33		
3684.99	-103	3686.253	TiII	(14)	$a^2F_{7/2}$-$z^2D_{5/2}$			33		
3687.65			unid					11		
3697.79			unid					4		
3706.07	-98	3707.271	TiII	(72)	$b^2D_{3/2}$-$y^2D_{3/2}$			18		
3709.69	-50	3710.301	FeI	(21)	a^5F_4-y^5F_3			9		id?
3715.36	-96	3716.545	VII	(15)	a^3H_6-z^3G_5			13		
3719.87	-91	3720.993	FeI	(5)	a^5D_4-z^5F_5			12		
3721.59	-90	3722.698	TiII	(13)	$a^2F_{5/2}$-$z^2F_{7/2}$			16		
3727.36	-106	3728.679	FeI	(21)	a^5F_3-y^5F_2			18		
3732.73	-88	3733.824	VII	(15)	a^3H_5-z^3G_4			12		
3734.73	-96	3735.926	FeI	(21)	a^5F_5-y^5F_5			27		
3736.95	-100	3738.194	FeI	(5)	a^5D_3-z^5F_4			26		
3741.51	-95	3742.699	TiII	(72)	$b^2D_{5/2}$-$y^2D_{5/2}$			29		
3743.31	-90	3744.426	FeI	(21)	a^5F_2-y^5F_1			5		
3745.61	-102	3746.875	VII	(15)	a^3H_4-z^3G_3			17		
3745.61	-81	3746.626	FeI	(5)	a^5D_2-z^5F_3			17		
3748.02	-105	3749.327	FeI	(5)	a^5D_1-z^5F_2			5		
3749.44	-89	3750.551	FeI	(21)	a^5F_4-y^5F_4			27		
3750.98	-77	3751.944	VII	(21)	b^3F_3-z^3F_3			3		
3757.77	-79	3758.756	TiII	(73)	$b^2D_{3/2}$-$z^2P_{3/2}$			31		
3757.77	-122	3759.301	FeI	(21)	a^5F_3-y^5F_3			31		
3759.35	-81	3760.364	TiII	(13)	$a^2F_{7/2}$-$z^2F_{7/2}$			3		bl.
3761.14	-100	3762.392	TiII	(13)	$a^2F_{5/2}$-$z^2F_{5/2}$			29		
3763.66	-95	3764.858	FeI	(21)	a^5F_2-y^5F_2			13		
3767.10	-93	3768.262	FeI	(21)	a^5F_1-y^5F_1			8		
3770.87	-94	3772.046	VII	(21)	b^3F_2-z^3F_2			11		
3774.24	-132	3775.896	FeI	(73)	a^5P_1-w^5D_1			9		bl.
3774.24			unid					9		
3776.01	-88	3777.124	TiII	(73)	$b^2D_{5/2}$-$z^2P_{3/2}$			5		
3787.90	-84	3788.956	FeI	(21)	a^5F_1-y^5F_2			9		
3794.82	-100	3796.080	FeI	(21)	a^5F_2-y^5F_3			3		
3813.05	-111	3814.464	TiII	(12)	$a^2F_{7/2}$-$z^4F_{7/2}$	7		5		
3814.38	-101	3815.667	TiII	(12)	$a^2F_{5/2}$-$z^4F_{3/2}$	14		21		
3815.66	-99	3816.923	FeI	(45)	a^3F_4-y^3D_3	7		6		
3820.25	-99	3821.509	FeI	(20)	a^5F_5-y^5D_4	13		18		
3824.18	-106	3825.529	FeI	(4)	a^5D_4-z^5D_3			2		
3825.75	-95	3826.966	FeI	(20)	a^5F_4-y^5D_3	8		15		
3827.71	-94	3828.909	FeI	(45)	a^3F_3-y^3D_2	4		7		bl.
3834.10	-95	3835.310	FeI	(20)	a^5F_3-y^5D_2	8		12		
3836.01	-91	3837.173	TiII	(12)	$a^2F_{7/2}$-$z^4F_{5/2}$	21		16		
3840.51	-79	3841.526	FeI	(20)	a^5F_2-y^5D_1	11		12		
3842.80	-105	3844.140	ScII	(1)	a^3D_2-z^1D_2	2		3		
3849.83	-96	3851.061	FeI	(20)	a^5F_1-y^5D_0	4		5		
3856.35			unid			5		4		
3859.75	-98	3861.005	FeI	(4)	a^5D_4-z^5D_4	7		10		
3863.57	-98	3864.836	FeI	(280)	a^3G_5-w^5G_4	2		2		id?
3865.41	-94	3866.619	FeI	(20)	a^5F_1-y^5D_1	2		2		
3872.38	-94	3873.599	FeI	(20)	a^5F_2-y^5D_2	2		3		
3878.41	-98	3879.672	FeI	(4)	a^5D_2-z^5D_1	7		10		
3886.37	-78	3887.383	FeI	(4)	a^5D_3-z^5D_3	5		8		
3895.85	-108	3897.259	VII	(9)	a^3P_0-z^5F_1	3		4		
3900.32	-103	3901.656	TiII	(34)	$a^2G_{9/2}$-$z^2G_{9/2}$	21		25		

Table 2. Continued.

λ_{obs} (Å)	Velocity (km/s)	λ_{lab} (Å)	Ion	Mult.	Transition[a]	I(mar00)	I(apr01)	I(nov01)	I(dec02)	Comment[b]
						(10^{-15} erg cm^{-2} s^{-1} arcsec^{-2})				
3903.05	-102	3904.374	VII	(11)	a^3P_2-z^5D_3	7		9		
3913.27	-100	3914.576	TiII	(34)	$a^2G_{7/2}$-$z^2G_{7/2}$	23		31		
3916.19	-102	3917.519	VII	(10)	a^3P_1-z^3D_2	5		7		
3932.39	-182	3934.777	CaII	(1)	4s $^2S_{1/2}$-4p $^2P^o_{3/2}$	10		19		
3951.84	-94	3953.083	VII	(10)	a^3P_2-z^3D_3	5		8		
3958.07			unid			1		1		
3967.27	-175	3969.592	CaII	(1)	4s $^2S_{1/2}$-4p $^2P^o_{1/2}$	19		29		
3991.21	-99	3992.530	[CrII]	(4F)	$a^6S_{5/2}$-$b^4D_{5/2}$	2		5		
3993.20	-86	3994.340	[CrII]	(4F)	$a^6S_{5/2}$-$b^4D_{1/2}$	8		8		
3993.20	-107	3994.620	[CrII]	(4F)	$a^6S_{5/2}$-$b^4D_{7/2}$	8		8		
3996.99	-95	3998.250	VII	(9)	a^3P_2-z^5F_3	4		6		
4005.44	-70	4006.373	FeI	(43)	a^3F_3-y^3F_2	7		9		
4005.44	-105	4006.838	VII	(32)	a^3G_5-z^3G_5	7		9		
4012.18	-100	4013.519	TiII	(11)	$a^2F_{5/2}$-$z^4G_{5/2}$	11		15		
4023.22	-97	4024.525	VII	(32)	a^3G_4-z^3G_4	4		6		
4024.97	-97	4026.269	TiII	(11)	$a^2F_{7/2}$-$z^4G_{7/2}$	7		9		
4028.14	-100	4029.481	TiII	(87)	$b^2G_{9/2}$-$y^2F_{7/2}$	7		11		
4035.54	-91	4036.767	VII	(32)	a^3G_3-z^3G_3	6		6		
4045.65	-97	4046.956	FeI	(43)	a^3F_4-y^3F_4	9		11		
4053.65	-98	4054.979	TiII	(87)	$b^2G_{7/2}$-$y^2F_{5/2}$	5		6		
4063.37	-101	4064.742	FeI	(43)	a^3F_3-y^3F_3	3	5	5		
4071.40	-110	4072.887	FeI	(43)	a^3F_2-y^3F_2	6	7	7		
4077.49	-101	4078.860	SrII	(1)	$a^2S_{1/2}$-$a^2P_{3/2}$	12	13	13		
4143.72	-95	4145.038	FeI	(43)	a^3F_3-y^3F_4	3	4	3		
4149.13	-102	4150.535	FeI	(694)	z^5F_5-e^7G_6	3	4	4		id?
4152.30	-105	4153.755	[CoII]	(–)	a^3F_4-b^3P_2	7	6	7		id?
4161.25	-105	4162.708	TiII	(21)	$a^2D_{5/2}$-$z^4D_{7/2}$	3	4	4		
4163.45	-99	4164.822	TiII	(105)	$b^2F_{7/2}$-$x^2D_{5/2}$	11	13	13		
4171.68	-101	4173.086	TiII	(105)	$b^2F_{5/2}$-$x^2D_{3/2}$	8	9	9		
4173.39	-95	4174.713	TiII	(21)	$a^2D_{5/2}$-$z^4D_{5/2}$	5	6	5		
4201.82	-99	4203.212	FeI	(42)	a^3F_4-z^3G_4	10	6	9		
4215.29	-101	4216.706	SrII	(1)	$a^2S_{1/2}$-$a^2P_{1/2}$	7	10	11		
4226.52	-99	4227.918	CaI	(2)	$4s^2$ $^1S_0$-4s4p $^1P^o_1$	11	12	12		
4246.49	-108	4248.018	ScII	(7)	a^1D_2-z^1D_2	19	25	17		
4271.55	-99	4272.961	FeI	(42)	a^3F_4-z^3G_5	8	9	8		
4289.89	-107	4291.426	TiII	(41)	$a^4P_{3/2}$-$z^4D_{5/2}$	56	36	35		
4293.81	-105	4295.307	TiII	(20)	$a^2D_{5/2}$-$z^2D_{5/2}$	22	25	26		
4293.81	-106	4295.332	FeI	(41)	a^3F_4-z^5G_4	22		26		
4299.75	-105	4301.259	TiII	(41)	$a^4P_{5/2}$-$z^4D_{7/2}$	48	64	65		
4301.66	-102	4303.124	TiII	(41)	$a^4P_{1/2}$-$z^4D_{3/2}$	13		14		
4305.24			unid				8	6		
4307.60	-103	4309.075	TiII	(41)	$a^4P_{3/2}$-$z^4D_{3/2}$	24	28	27		
4307.60	-105	4309.114	FeI	(42)	a^3F_3-z^3G_4	24		27		
4312.64	-100	4314.076	TiII	(41)	$a^4P_{5/2}$-$z^4D_{5/2}$	20	23	24		
4314.07	-85	4315.296	ScII	(15)	a^3F_4-z^3D_3	28	36	29		
4320.51	-100	4321.947	ScII	(15)	a^3F_3-z^3D_2	39	29	26		
4324.84	-95	4326.212	ScII	(15)	a^3F_2-z^3D_1	14	28	28		
4324.84	-181	4327.453	[NiII]	(4F)	$a^2D_{5/2}$-$a^4P_{5/2}$		25	28		
4330.31	-80	4331.463	TiII	(93)	$b^2P_{1/2}$-$y^2D_{3/2}$			4		
4337.68	-101	4339.135	TiII	(20)	$a^2D_{3/2}$-$z^2D_{3/2}$		31	30		
4341.39	-83	4342.585	TiII	(32)	$a^2G_{7/2}$-$z^2D_{5/2}$		23	14		
4367.40	-102	4368.886	TiII	(104)	$b^2F_{7/2}$-$y^2G_{9/2}$		4	4		
4374.35	-92	4375.686	ScII	(14)	a^3F_4-z^3F_4		23	14		

Table 2. Continued.

λ_{obs} (Å)	Velocity (km/s)	λ_{lab} (Å)	Ion	Mult.	Transition[a]	I(mar00)	I(apr01)	I(nov01)	I(dec02)	Comment[b]
						(10^{-15} erg cm^{-2} s^{-1} arcsec^{-2})				
4383.33	-99	4384.776	FeI	(41)	a^3F_4-z^5G_5		17	14		
4394.80	-100	4396.268	TiII	(19)	$a^2D_{5/2}$-$z^2F_{7/2}$		46	43		
4399.80	-83	4401.008	TiII	(51)	$a^2P_{3/2}$-$z^4D_{5/2}$		29	27		
4399.80	-125	4401.625	ScII	(14)	a^3F_3-z^3F_3			27		
4404.65	-91	4405.987	FeI	(41)	a^3F_3-z^5G_4		8	6		
4415.16	-82	4416.362	FeI	(41)	a^3F_2-z^5G_3		50	44		
4415.16	-111	4416.797	ScII	(14)	a^3F_2-z^3F_2			44		
4417.43	-104	4418.960	TiII	(40)	$a^4P_{3/2}$-$z^2D_{5/2}$		43	29		
4427.25			unid				2	2		
4443.61	-97	4445.042	TiII	(19)	$a^2D_{3/2}$-$z^2F_{5/2}$		40	40		
4450.39	-91	4451.731	TiII	(19)	$a^2D_{5/2}$-$z^2F_{5/2}$		14	14		
4464.25	-98	4465.703	TiII	(40)	$a^4P_{1/2}$-$z^2D_{3/2}$		8	5		
4468.31	-97	4469.761	TiII	(31)	$a^2G_{9/2}$-$z^2F_{7/2}$		47	45		
4482.13	-93	4483.510	FeI	(68)	a^5P_1-x^5D_2		2	2		
4501.08	-97	4502.536	TiII	(31)	$a^2G_{7/2}$-$z^2F_{5/2}$		41	39		
4533.73	-100	4535.240	TiII	(50)	$a^2P_{3/2}$-$z^2D_{5/2}$		41	39		
4549.45	-95	4550.892	TiII	(84)	$a^2H_{11/2}$-$y^2G_{9/2}$		40	41		
4563.54	-99	4565.040	TiII	(50)	$a^2P_{1/2}$-$z^2D_{3/2}$		40	40		
4571.70	-102	4573.249	TiII	(84)	$a^2H_{9/2}$-$y^2G_{7/2}$		46	42		
4580.60	-97	4582.088	[CrII]	(3F)	$a^6S_{5/2}$-$a^4P_{3/2}$		13	12		
4580.60	-101	4582.145	[CrII]	(3F)	$a^6S_{5/2}$-$a^4P_{1/2}$			12		
4580.60	-119	4582.422	[CrII]	(3F)	$a^6S_{5/2}$-$a^4P_{1/2}$			12		
4589.77	-96	4591.244	TiII	(50)	$a^2P_{3/2}$-$z^2D_{3/2}$		9	8		
4622.89	-39	4623.490	[FeI]	(21F)	a^5F_3-b^3D_2			6		
4670.19	-98	4671.714	ScII	(24)	b^1D_2-z^1F_3			4		
4708.47	-97	4709.983	TiII	(49)	$a^2P_{3/2}$-$z^2F_{5/2}$			2		id?. bl. abs
4747.17			unid					9		
4763.86			unid					4		
4779.51	-114	4781.321	TiII	(92)	$b^2P_{1/2}$-$z^2S_{1/2}$			7		
4802.32			unid					7		
4804.82	-101	4806.428	TiII	(92)	$b^2P_{3/2}$-$z^2S_{1/2}$			7		
4843.00	-105	4844.701	[FeI]	(4F)	a^5D_4-b^3F2_4	2	3	4		id?
4916.68	-96	4918.247	[TiII]	(23F)	$a^2F_{5/2}$-$c^2D_{3/2}$	9	9	11		
4925.63	-101	4927.288	[TiII]	(23F)	$a^2F_{7/2}$-$c^2D_{5/2}$	6	19	20		
4982.44	-106	4984.205	[TiII]	(23F)	$a^2F_{7/2}$-$c^2D_{3/2}$	1	1	2		
5030.86	-93	5032.424	ScII	(23)	b^1D_2-z^3P_1	3	5	5		
5128.89	-99	5130.581	TiII	(86)	$b^2G_{9/2}$-$z^2G_{9/2}$			3		
5153.70	-105	5155.506	TiII	(70)	$b^2D_{3/2}$-$z^2D_{5/2}$			5		
5188.38	-101	5190.125	TiII	(70)	$b^2D_{5/2}$-$z^2D_{5/2}$			14		
5211.25	-100	5212.987	TiII	(103)	$b^2F_{7/2}$-$y^2F_{7/2}$			1		
5226.00	-115	5227.998	TiII	(70)	$b^2D_{3/2}$-$z^2D_{3/2}$			15		
5239.54	-99	5241.272	ScII	(26)	a^1S_0-z^1P_1			3		
5253.20			unid					1		
5303.74			unid					3		
5327.73	-101	5329.520	FeI	(15)	a^5F_4-z^5D_3			2		
5371.29	-95	5372.983	FeI	(15)	a^5F_3-z^5D_2			1		
5394.10	-90	5395.713	[MnII]	(9F)	a^5D_4-b^5D_2			6		
5394.10	-121	5396.266	[MnII]	(9F)	a^5D_4-b^5D_3			6		
5414.34	-121	5416.528	[MnII]	(9F)	a^5D_4-b^5D_4			18		bl.
5418.60	-92	5420.257	TiII	(69)	$b^2D_{5/2}$-$z^2F_{5/2}$			3		
5470.63			unid					7		
5472.97	-104	5474.872	[MnII]	(9F)	a^5D_3-b^5D_2			9		
5472.97	-135	5475.440	[MnII]	(9F)	a^5D_3-b^5D_3			9		

Table 2. Continued.

λ_{obs} (Å)	Velocity (km/s)	λ_{lab} (Å)	Ion	Mult.	Transition[a]	I(mar00)	I(apr01)	I(nov01)	I(dec02)	Comment[b]
						(10^{-15} erg cm^{-2} s^{-1} arcsec^{-2})				
5494.38	-105	5496.302	[MnII]	(9F)	a^5D_3-b^5D_4			7		
5526.53	-97	5528.325	ScII	(31)	a^1G_4-z^1F_3			14		
5559.85			unid					4		
5599.35			unid					1		
5639.42	-91	5641.119	[FeI]	(2F)	a^5D_4-a^5P_2			12		
5639.42	-168	5642.567	ScII	(29)	a^3P_1-z^3P_2			12		bl.
5657.74	-92	5659.466	ScII	(29)	a^3P_2-z^3P_2			8		
5657.74	-116	5659.931	ScII	(29)	a^3P_0-z^3P_1			8		
5696.03	-101	5697.949	[FeI]	(2F)	a^5D_4-a^5P_3			11		
5708.73	-96	5710.551	[FeI]	(2F)	a^5D_3-a^5P_1			6		
5804.07	-103	5806.063	[FeI]	(2F)	a^5D_2-a^5P_1			4		
5834.42	-95	5836.266	[FeI]	(2F)	a^5D_3-a^5P_3			10		
5889.25	-119	5891.583	NaI	(1)	$3s\ ^2S_{1/2}$-$3p\ ^2P^o_{3/2}$			77		
5895.29	-115	5897.558	NaI	(1)	$3s\ ^2S_{1/2}$-$3p\ ^2P^o_{1/2}$			84		
5934.02	-104	5936.067	[FeI]	(2F)	a^5D_2-a^5P_3			4		
5936.54	-106	5938.647	[FeI]	(2F)	a^5D_1-a^5P_2			3		
6077.80	-87	6079.567	[TiII]	(26F)	$a^2D_{5/2}$-$c^2D_{5/2}$			3		
6124.37	-95	6126.311	[TiII]	(22F)	$a^2F_{5/2}$-$b^2F_{5/2}$			11		
6147.20	-83	6148.896	[TiII]	(22F)	$a^2F_{5/2}$-$b^2F_{7/2}$			3		
6151.75	-91	6153.623	[TiII]	(26F)	$a^2D_{3/2}$-$c^2D_{3/2}$			5		
6160.44			unid					2		
6219.08			unid					2		
6227.10	-91	6228.990	[TiII]	(22F)	$a^2F_{7/2}$-$b^2F_{5/2}$			2		
6250.37	-95	6252.341	[TiII]	(22F)	$a^2F_{7/2}$-$b^2F_{7/2}$			18		
6279.56	-92	6281.490	ScII	(28)	a^3P_1-z^3D_2			2		
6410.66	-105	6412.900	[MnII]	(8F)	a^5D_4-a^5P_2			6		
6422.96	-106	6425.224	[MnII]	(8F)	a^5D_4-a^5P_3			7		
6509.14	-106	6511.434	[MnII]	(8F)	a^5D_3-a^5P_1	7	7	9		
6519.09	-101	6521.281	[CoII]	(–)	b^3F_4-b^1G_4	4	4	6		
6535.55	-103	6537.786	[MnII]	(8F)	a^5D_3-a^5P_3	6	6	5		
6647.03	-88	6648.980	[TiII]	(8F)	$a^4F_{7/2}$-$b^2G_{7/2}$	2	2	1		
6650.29	-105	6652.610	[TiII]	(8F)	$a^4F_{7/2}$-$b^2G_{9/2}$	2	2	2		
6656.38	-99	6658.570	[MnII]	(8F)	a^5D_1-a^5P_2	1	2	2		
6666.25	-109	6668.670	[NiII]	(2F)	$a^2D_{5/2}$-$a^2F_{5/2}$	52	45	51		
6725.49	-97	6727.670	[TiII]	(8F)	$a^4F_{9/2}$-$b^2G_{9/2}$	4	5	6		
6738.23	-89	6740.230	[SrII]	(1F)	$a^2S_{1/2}$-$a^2D_{5/2}$	3	4	4		
6760.48	-89	6762.484	[FeI]	(15F)	a^5F_5-a^3G_5	2	3	4		
6791.25	-93	6793.350	[NiII]	(8F)	$a^4F_{5/2}$-$a^4P_{1/2}$	0.5	1	1		
6813.94	-66	6815.450	[NiII]	(8F)	$a^4F_{5/2}$-$a^4P_{3/2}$	5	4	7		
6836.79	-90	6838.838	[FeI]	(15F)	a^5F_4-a^3G_4	1	2	1		
6849.33	-126	6852.215	[MnII]	(2F)	a^7S_3-a^5D_3	0.5	1	1		
6868.05	-88	6870.070	[SrII]	(1F)	$a^2S_{1/2}$-$a^2D_{3/2}$	1	3	3		
6923.30	-106	6925.736	[CoII]	(–)	b^3F_3-b^1G_4	1	2	2		
6931.35	-126	6934.270	[CoII]	(3F)	a^5F_5-a^5P_3	5	6	8		
6971.58	-104	6974.000	[FeI]	(15F)	a^5F_4-a^3G_5	1	0.5	1		
6977.73	-114	6980.380	[MnII]	(2F)	a^7S_3-a^5D_4	0.5	1	1		
6998.68			unid			2	2	2		
7004.46	-116	7007.180	[FeI]	(15F)	a^5F_3-a^3G_4	1	2	2		
7099.61	-110	7102.208	[CoII]	(–)	a^3P_1-a^3D_3	4	4	5		id?
7256.06	-74	7257.860	[NiII]	(8F)	$a^4F_{7/2}$-$a^4P_{5/2}$	6	8	9		
7274.08	-103	7276.590	[CoII]	(3F)	a^5F_4-a^5P_3		2	2		bl
7290.79	-111	7293.480	[CaII]	(1F)	$4s\ ^2S_{1/2}$-$3d\ ^2D_{5/2}$	35	43	46		
7323.11	-115	7325.910	[CaII]	(1F)	$4s\ ^2S_{1/2}$-$3d\ ^2D_{3/2}$	61	62	73		

Table 2. Continued.

λ_{obs} (Å)	Velocity (km/s)	λ_{lab} (Å)	Ion	Mult.	Transition[a]	I(mar00)	I(apr01)	I(nov01)	I(dec02)	Comment[b]
						(10^{-15} erg cm^{-2} s^{-1} arcsec^{-2})				
7331.89	-89	7334.077	[VII]	(4F)	a^5D_2-a^5P_3	7	7	8		
7343.90	-87	7346.030	[VII]	(12F)	a^5F_3-b^3G_4		2	2		
7353.97	-74	7355.792	[VII]	(4F)	a^5D_0-a^5P_2	3	4	5		
7377.22	-112	7379.970	[NiII]	(2F)	$a^2D_{5/2}$-$a^2F_{7/2}$	188	170	213		
7411.22	-100	7413.690	[NiII]	(2F)	$a^2D_{3/2}$-$a^2F_{5/2}$	109	83	98		
7426.27			unid			4	5	7		
7430.71			unid			2	3	4		
7458.61	-110	7461.350	[VII]	(4F)	a^5D_4-a^5P_3	23	22	24		
7458.61	-162	7462.648	[VII]	(3F)	a^5D_3-b^3F_4	23		24		
7476.97	-94	7479.321	[VII]	(12F)	a^5F_5-b^3G_5	2	4	5		
7497.38	-95	7499.749	[VII]	(3F)	a^5D_3-b^3F_3	4	4	4		
7514.82	-94	7517.180	[VII]	(4F)	a^5D_3-a^5P_1	8	10	10		
7533.52	-96	7535.937	[VII]	(3F)	a^5D_4-b^3F_4	7	6	8		
7541.65	-94	7544.026	[VII]	(4F)	a^5D_4-a^5P_2	12	12	15		
7546.96	-113	7549.797	[MnII]	(7F)	a^5D_4-a^5G_5	5	5	5		
7546.96	-121	7549.997	[VII]	(–)	a^5P_2-a^1F_3	5		5		
7560.51	-119	7563.501	[MnII]	(7F)	a^5D_4-a^5G_6	37	40	39		
7664.71			unid					13		
7702.69	-117	7705.686	[MnII]	(7F)	a^5D_3-a^5G_5			12		
7749.18			unid					4		
7805.16	-111	7808.041	[MnII]	(7F)	a^5D_2-a^5G_3			7		
7805.16	-92	7807.566	[MnII]	(7F)	a^5D_2-a^5G_2			7		
7808.06	-115	7811.048	[MnII]	(7F)	a^5D_2-a^5G_4			6		
7878.66	-105	7881.401	[MnII]	(7F)	a^5D_1-a^5G_2			8		
7915.30	-119	7918.452	[TiII]	(6F)	$a^4F_{3/2}$-$b^2D_{3/2}$			3		
7976.40	-56	7977.897	[TiII]	(6F)	$a^4F_{5/2}$-$b^2D_{3/2}$			6		
7976.40	-110	7979.330	[TiII]	(6F)	$a^4F_{7/2}$-$b^2D_{5/2}$			6		
7999.22	-115	8002.279	[CrII]	(1F)	$a^6S_{5/2}$-$a^6D_{9/2}$			66		
8050.43			unid					3		
8124.09	-127	8127.531	[CrII]	(1F)	$a^6S_{5/2}$-$a^6D_{7/2}$			85		
8228.60	-121	8231.930	[CrII]	(1F)	$a^6S_{5/2}$-$a^6D_{5/2}$			75		
8260.96	-90	8263.438	[ScII]	(3F)	a^3D_1-a^3P_1			2		
8270.91	-96	8273.557	[ScII]	(3F)	a^3D_2-a^3P_2			3		
8300.15	-113	8303.270	[NiII]	(2F)	$a^2D_{3/2}$-$a^2F_{7/2}$			10		
8307.20	-129	8310.770	[CrII]	(1F)	$a^6S_{5/2}$-$a^6D_{3/2}$			57		
8326.54	-85	8328.905	[ScII]	(3F)	a^3D_2-a^3P_0			2		
8332.81	-100	8335.590	[TiII]	(–)	$a^2F_{5/2}$-$b^2P_{3/2}$			2		
8347.07	-101	8349.870	[FeI]	(1F)	a^5D_4-a^3F_4			5		
8347.07	-90	8349.570	[ScII]	(3F)	a^3D_3-a^3P_2			5		
8356.68	-117	8359.939	[CrII]	(1F)	$a^6S_{5/2}$-$a^6D_{1/2}$			26		
8409.61	-98	8412.354	[TiII]	(–)	$a^2F_{5/2}$-$b^2P_{1/2}$			7		
8470.28	-110	8473.399	[VII]	(2F)	a^5D_2-a^3P_2			7		id? bl. HI
8497.15	-113	8500.358	CaII	(2)	$3d\,^2D_{3/2}$-$4p\,^2P^o_{3/2}$			1		
8524.19	-99	8526.997	[TiII]	(–)	$a^2F_{5/2}$-$b^2P_{3/2}$			14		
8529.22	-95	8531.906	[TiII]	(15F)	$b^4F_{3/2}$-$b^2D_{3/2}$			11		
8540.98	-121	8544.438	CaII	(2)	$3d\,^2D_{5/2}$-$4p\,^2P^o_{3/2}$			37		
8565.44	-104	8568.400	[TiII]	(15F)	$b^4F_{7/2}$-$b^2D_{5/2}$			6		
8584.56	-103	8587.494	[TiII]	(15F)	$b^4F_{5/2}$-$b^2D_{3/2}$			5		
8661.10	-94	8663.807	[TiII]	(15F)	$b^4F_{9/2}$-$b^2D_{5/2}$			53		
8661.10	-116	8664.452	[TiII]	(15F)	$b^4F_{7/2}$-$b^2D_{3/2}$			53		
8661.10	-118	8664.520	CaII	(2)	$3d\,^2D_{3/2}$-$4p\,^2P^o_{1/2}$			53		
8674.12			unid					2		
8698.34			unid					2		

Table 2. Continued.

λ_{obs} (Å)	Velocity (km/s)	λ_{lab} (Å)	Ion	Mult.	Transition[a]	I(mar00)	I(apr01)	I(nov01)	I(dec02)	Comment[b]
						(10^{-15} erg cm^{-2} s^{-1} arcsec^{-2})				
8726.82	-93	8729.523	[CI]	(3F)	$2p^2\ ^1D_2$-$2p^2\ ^1S_0$			15		
8762.84	-97	8765.679	[VII]	(2F)	a^5D_2-a^3P_1			7		
8806.31			unid					4		
8878.60	-94	8881.373	[VII]	(2F)	a^5D_1-a^3P_0			5		
9334.98	-110	9338.400	[CoII]	(1F)	a^3F_4-b^3F_3	2		6		
9341.82			unid			1		4		
9405.00	-107	9408.356	[TiII]	(21F)	$a^2F_{5/2}$-$b^2G_{9/2}$	6		3		
9638.81	-95	9641.850	[CoII]	(1F)	a^3F_3-b^3F_2	4		4		
9642.18	-90	9645.089	[TiII]	(21F)	$a^2F_{7/2}$-$b^2G_{7/2}$	1		0.4		
9649.74	-92	9652.716	[TiII]	(21F)	$a^2F_{7/2}$-$b^2G_{9/2}$	1		2		
9824.56	-69	9826.822	[CI]	(1F)	$2p^2\ ^3P_1$-$2p^2\ ^1D_2$	0.3		1		
9850.24	-83	9852.965	[CI]	(1F)	$2p^2\ ^3P_2$-$2p^2\ ^1D_2$	2		2		
10066.4	-100	10069.740	[TiII]	(5F)	$a^4F_{5/2}$-$b^4P_{5/2}$	5		3		
10066.4	-103	10069.850	[TiII]	(5F)	$a^4F_{3/2}$-$b^4P_{3/2}$	5		3		
10125.73	-90	10128.770	[TiII]	(5F)	$a^4F_{3/2}$-$b^4P_{1/2}$	5		7		

[a] The configurations in complex spectra are replaced by symbols using the system introduced by Moore (1945). For each ion the lowest even parity *LS*-term of each type is assigned the prefix a, the next b, and so on. Similarily, the odd terms are assigned the prefixes z,y,x etc. For example, the lowest even ^{4}D in Fe II is written as a^{4}D, the second b^{4}D and the lowest odd ^{4}D is marked z^{4}D. This system is not applied to the light elements, where the odd terms are marked with the superscript ^{o}, for example $^3P^o_1$.

[b] Abbreviations used in the comment column:
bl.=lines blended by features not included in the list.
bl.abs=lines being partially blended by an absorption feature.
bl.HP=lines affected by hot pixels.
id?=identification uncertain.
Filament lines with more than one plausible identification are listed with the same measured wavelength, λ_{obs}, in column 1 but are not explicitly marked as blends in the Comment column.

Table 3. Spectral lines observed in the Sr-filament of η Car in the wavelength region 2480-10140 Å. The lines are primarily sorted by ion and within each ion by excitation energy.

Velocity (km/s)	λ_{lab} (Å)	Ion	Mult.	Transition	E_{exc} (eV)
-69	9826.822	[CI]	(1F)	$2p^2\ ^3P_1$-$2p^2\ ^1D_2$	1.3
-83	9852.965	[CI]	(1F)	$2p^2\ ^3P_2$-$2p^2\ ^1D_2$	1.3
-93	8729.523	[CI]	(3F)	$2p^2\ ^1D_2$-$2p^2\ ^1S_0$	2.7
-115	5897.558	NaI	(1)	$3s\ ^2S_{1/2}$-$3p\ ^2P^o_{1/2}$	2.1
-119	5891.583	NaI	(1)	$3s\ ^2S_{1/2}$-$3p\ ^2P^o_{3/2}$	2.1
-95	2852.964	MgI	(uv1)	$3s^2\ ^1S_0$-$3s3p\ ^1P^o_1$	4.3
-99	2669.949	AlII	(uv1)	$3s^2\ ^1S_0$-$3s3p\ ^3P^o_1$	4.6
-99	4227.918	CaI	(2)	$4s^2\ ^1S_0$-$4s4p\ ^1P^o_1$	2.9
-175	3969.592	CaII	(1)	$4s\ ^2S_{1/2}$-$4p\ ^2P^o_{1/2}$	3.1
-118	8664.520	CaII	(2)	$3d\ ^2D_{3/2}$-$4p\ ^2P^o_{1/2}$	3.1
-182	3934.777	CaII	(1)	$4s\ ^2S_{1/2}$-$4p\ ^2P^o_{3/2}$	3.2
-113	8500.358	CaII	(2)	$3d\ ^2D_{3/2}$-$4p\ ^2P^o_{3/2}$	3.2
-121	8544.438	CaII	(2)	$3d\ ^2D_{5/2}$-$4p\ ^2P^o_{3/2}$	3.2
-115	7325.910	[CaII]	(1F)	$4s\ ^2S_{1/2}$-$3d\ ^2D_{3/2}$	1.7
-111	7293.480	[CaII]	(1F)	$4s\ ^2S_{1/2}$-$3d\ ^2D_{5/2}$	1.7
-12	3360.643	ScII	(4)	a^3D_2-z^3P_2	3.0
-105	3844.140	ScII	(1)	a^3D_2-z^1D_2	3.2
-108	4248.018	ScII	(7)	a^1D_2-z^1D_2	3.2
-111	4416.797	ScII	(14)	a^3F_2-z^3F_2	3.4
-125	4401.625	ScII	(14)	a^3F_3-z^3F_3	3.4
-95	3643.822	ScII	(2)	a^3D_1-z^3F_2	3.4
-95	3652.835	ScII	(2)	a^3D_2-z^3F_2	3.4
-87	3631.777	ScII	(2)	a^3D_2-z^3F_3	3.4
-89	3646.350	ScII	(2)	a^3D_3-z^3F_3	3.4
-92	4375.686	ScII	(14)	a^3F_4-z^3F_4	3.5
-95	4326.212	ScII	(15)	a^3F_2-z^3D_1	3.5
-100	4321.947	ScII	(15)	a^3F_3-z^3D_2	3.5
-85	4315.296	ScII	(15)	a^3F_4-z^3D_3	3.5
-101	3614.860	ScII	(2)	a^3D_3-z^3F_4	3.5
-92	6281.490	ScII	(28)	a^3P_1-z^3D_2	3.5
-86	3581.947	ScII	(3)	a^3D_1-z^3D_1	3.5
-90	3568.715	ScII	(3)	a^3D_1-z^3D_2	3.5
-76	3590.656	ScII	(3)	a^3D_2-z^3D_1	3.5
-93	3577.361	ScII	(3)	a^3D_2-z^3D_2	3.5
-107	3559.548	ScII	(3)	a^3D_2-z^3D_3	3.5
-146	3591.499	ScII	(3)	a^3D_3-z^3D_2	3.5
-101	3573.546	ScII	(3)	a^3D_3-z^3D_3	3.5
-116	5659.931	ScII	(29)	a^3P_0-z^3P_1	3.7
-168	5642.567	ScII	(29)	a^3P_1-z^3P_2	3.7
-92	5659.466	ScII	(29)	a^3P_2-z^3P_2	3.7
-154	3362.231	ScII	(4)	a^3D_1-z^3P_1	3.7
-80	3369.904	ScII	(4)	a^3D_2-z^3P_1	3.7
-83	3373.117	ScII	(4)	a^3D_3-z^3P_2	3.7
-123	3536.725	ScII	(11)	a^1D_2-z^1P_1	3.8
-93	5032.424	ScII	(23)	b^1D_2-z^3P_1	3.8
-99	5241.272	ScII	(26)	a^1S_0-z^1P_1	3.8
-99	3354.688	ScII	(12)	a^1D_2-z^1F_3	4.0
-98	4671.714	ScII	(24)	b^1D_2-z^1F_3	4.0
-97	5528.325	ScII	(31)	a^1G_4-z^1F_3	4.0
-93	2563.958	ScII	(uv1)	a^3D_1-y^3P_0	4.8
-288	2560.996	ScII	(uv1)	a^3D_2-y^3P_1	4.8

Table 3. continued.

Velocity (km/s)	λ_{lab} (Å)	Ion	Mult.	Transition	E_{exc} (eV)
-83	2541.585	ScII	(uv1)	a^3D_1-y^3P_2	4.9
-105	2545.967	ScII	(uv1)	a^3D_2-y^3P_2	4.9
-93	2553.120	ScII	(uv1)	a^3D_3-y^3P_2	4.9
-90	8263.438	[ScII]	(3F)	a^3D_1-a^3P_1	1.5
-85	8328.905	[ScII]	(3F)	a^3D_2-a^3P_0	1.5
-96	8273.557	[ScII]	(3F)	a^3D_2-a^3P_2	1.5
-90	8349.570	[ScII]	(3F)	a^3D_3-a^3P_2	1.5
-142	3384.740	TiII	(1)	$a^4F_{3/2}$-$z^4G_{5/2}$	3.7
-141	3373.769	TiII	(1)	$a^4F_{5/2}$-$z^4G_{7/2}$	3.7
-105	3410.799	TiII	(1)	$a^4F_{7/2}$-$z^4G_{5/2}$	3.7
-104	3388.819	TiII	(1)	$a^4F_{7/2}$-$z^4G_{7/2}$	3.7
-150	3362.184	TiII	(1)	$a^4F_{7/2}$-$z^4G_{9/2}$	3.7
-140	3350.371	TiII	(1)	$a^4F_{9/2}$-$z^4G_{11/2}$	3.7
-122	3381.250	TiII	(1)	$a^4F_{9/2}$-$z^4G_{9/2}$	3.7
-100	4013.519	TiII	(11)	$a^2F_{5/2}$-$z^4G_{5/2}$	3.7
-97	4026.269	TiII	(11)	$a^2F_{7/2}$-$z^4G_{7/2}$	3.7
-103	3492.065	TiII	(6)	$b^4F_{3/2}$-$z^4G_{5/2}$	3.7
-99	3478.183	TiII	(6)	$b^4F_{5/2}$-$z^4G_{7/2}$	3.7
-103	3462.486	TiII	(6)	$b^4F_{7/2}$-$z^4G_{9/2}$	3.7
-105	3445.301	TiII	(6)	$b^4F_{9/2}$-$z^4G_{11/2}$	3.7
-123	3395.554	TiII	(63)	$b^4P_{5/2}$-$y^2D_{5/2}$	3.7
-101	3815.667	TiII	(12)	$a^2F_{5/2}$-$z^4F_{3/2}$	3.8
-91	3837.173	TiII	(12)	$a^2F_{7/2}$-$z^4F_{5/2}$	3.8
-153	3230.130	TiII	(2)	$a^4F_{3/2}$-$z^4F_{5/2}$	3.8
-87	3239.979	TiII	(2)	$a^4F_{5/2}$-$z^4F_{5/2}$	3.8
-98	3253.855	TiII	(2)	$a^4F_{7/2}$-$z^4F_{5/2}$	3.8
-148	3242.930	TiII	(66)	$b^4P_{3/2}$-$y^4D_{3/2}$	3.8
-77	3341.320	TiII	(7)	$b^4F_{3/2}$-$z^4F_{3/2}$	3.8
-101	3327.734	TiII	(7)	$b^4F_{3/2}$-$z^4F_{5/2}$	3.8
-90	3349.811	TiII	(7)	$b^4F_{5/2}$-$z^4F_{3/2}$	3.8
-101	3336.157	TiII	(7)	$b^4F_{5/2}$-$z^4F_{5/2}$	3.8
-125	3347.708	TiII	(7)	$b^4F_{7/2}$-$z^4F_{5/2}$	3.8
-111	3814.464	TiII	(12)	$a^2F_{7/2}$-$z^4F_{7/2}$	3.9
-100	3762.392	TiII	(13)	$a^2F_{5/2}$-$z^2F_{5/2}$	3.9
-90	3722.698	TiII	(13)	$a^2F_{5/2}$-$z^2F_{7/2}$	3.9
-81	3760.364	TiII	(13)	$a^2F_{7/2}$-$z^2F_{7/2}$	3.9
-102	3686.238	TiII	(14)	$a^2F_{5/2}$-$z^2D_{3/2}$	3.9
-97	4445.042	TiII	(19)	$a^2D_{3/2}$-$z^2F_{5/2}$	3.9
-91	4451.731	TiII	(19)	$a^2D_{5/2}$-$z^2F_{5/2}$	3.9
-100	4396.268	TiII	(19)	$a^2D_{5/2}$-$z^2F_{7/2}$	3.9
-119	3223.774	TiII	(2)	$a^4F_{5/2}$-$z^4F_{7/2}$	3.9
-139	3237.512	TiII	(2)	$a^4F_{7/2}$-$z^4F_{7/2}$	3.9
-122	3217.992	TiII	(2)	$a^4F_{7/2}$-$z^4F_{9/2}$	3.9
-103	3255.186	TiII	(2)	$a^4F_{9/2}$-$z^4F_{7/2}$	3.9
-101	4339.135	TiII	(20)	$a^2D_{3/2}$-$z^2D_{3/2}$	3.9
-97	4502.536	TiII	(31)	$a^2G_{7/2}$-$z^2F_{5/2}$	3.9
-97	4469.761	TiII	(31)	$a^2G_{9/2}$-$z^2F_{7/2}$	3.9
-98	4465.703	TiII	(40)	$a^4P_{1/2}$-$z^2D_{3/2}$	3.9
-97	4709.983	TiII	(49)	$a^2P_{3/2}$-$z^2F_{5/2}$	3.9
-99	4565.040	TiII	(50)	$a^2P_{1/2}$-$z^2D_{3/2}$	3.9
-96	4591.244	TiII	(50)	$a^2P_{3/2}$-$z^2D_{3/2}$	3.9
-92	5420.257	TiII	(69)	$b^2D_{5/2}$-$z^2F_{5/2}$	3.9
-102	3318.978	TiII	(7)	$b^4F_{5/2}$-$z^4F_{7/2}$	3.9

Table 3. continued.

Velocity (km/s)	λ_{lab} (Å)	Ion	Mult.	Transition	E_{exc} (eV)
-101	3330.411	TiII	(7)	$b^4F_{7/2}$-$z^4F_{7/2}$	3.9
-101	3309.757	TiII	(7)	$b^4F_{7/2}$-$z^4F_{9/2}$	3.9
-80	3344.726	TiII	(7)	$b^4F_{9/2}$-$z^4F_{7/2}$	3.9
-103	3323.897	TiII	(7)	$b^4F_{9/2}$-$z^4F_{9/2}$	3.9
-115	5227.998	TiII	(70)	$b^2D_{3/2}$-$z^2D_{3/2}$	3.9
-76	3162.136	TiII	(10)	$b^4F_{3/2}$-$z^4D_{1/2}$	4.0
-98	3155.118	TiII	(10)	$b^4F_{3/2}$-$z^4D_{3/2}$	4.0
-128	3162.689	TiII	(10)	$b^4F_{5/2}$-$z^4D_{3/2}$	4.0
-103	3686.253	TiII	(14)	$a^2F_{7/2}$-$z^2D_{5/2}$	4.0
-105	4295.307	TiII	(20)	$a^2D_{5/2}$-$z^2D_{5/2}$	4.0
-83	4342.585	TiII	(32)	$a^2G_{7/2}$-$z^2D_{5/2}$	4.0
-104	4418.960	TiII	(40)	$a^4P_{3/2}$-$z^2D_{5/2}$	4.0
-102	4303.124	TiII	(41)	$a^4P_{1/2}$-$z^4D_{3/2}$	4.0
-103	4309.075	TiII	(41)	$a^4P_{3/2}$-$z^4D_{3/2}$	4.0
-87	3067.245	TiII	(5)	$a^4F_{3/2}$-$z^4D_{3/2}$	4.0
-116	3076.123	TiII	(5)	$a^4F_{5/2}$-$z^4D_{3/2}$	4.0
-100	4535.240	TiII	(50)	$a^2P_{3/2}$-$z^2D_{5/2}$	4.0
-105	5155.506	TiII	(70)	$b^2D_{3/2}$-$z^2D_{5/2}$	4.0
-101	5190.125	TiII	(70)	$b^2D_{5/2}$-$z^2D_{5/2}$	4.0
-115	3153.172	TiII	(10)	$b^4F_{5/2}$-$z^4D_{5/2}$	4.1
-121	3163.488	TiII	(10)	$b^4F_{7/2}$-$z^4D_{5/2}$	4.1
-109	3169.449	TiII	(10)	$b^4F_{9/2}$-$z^4D_{7/2}$	4.1
-99	3597.078	TiII	(15)	$a^2F_{7/2}$-$z^4D_{5/2}$	4.1
-95	4174.713	TiII	(21)	$a^2D_{5/2}$-$z^4D_{5/2}$	4.1
-105	4162.708	TiII	(21)	$a^2D_{5/2}$-$z^4D_{7/2}$	4.1
-107	4291.426	TiII	(41)	$a^4P_{3/2}$-$z^4D_{5/2}$	4.1
-100	4314.076	TiII	(41)	$a^4P_{5/2}$-$z^4D_{5/2}$	4.1
-105	4301.259	TiII	(41)	$a^4P_{5/2}$-$z^4D_{7/2}$	4.1
-74	3067.119	TiII	(5)	$a^4F_{5/2}$-$z^4D_{5/2}$	4.1
-134	3079.551	TiII	(5)	$a^4F_{7/2}$-$z^4D_{5/2}$	4.1
-122	3073.015	TiII	(5)	$a^4F_{7/2}$-$z^4D_{7/2}$	4.1
-134	3088.934	TiII	(5)	$a^4F_{9/2}$-$z^4D_{7/2}$	4.1
-83	4401.008	TiII	(51)	$a^2P_{3/2}$-$z^4D_{5/2}$	4.1
-124	3342.841	TiII	(16)	$a^2F_{5/2}$-$z^2G_{7/2}$	4.3
-89	3373.181	TiII	(16)	$a^2F_{7/2}$-$z^2G_{7/2}$	4.3
-107	3350.000	TiII	(16)	$a^2F_{7/2}$-$z^2G_{9/2}$	4.3
-100	3914.576	TiII	(34)	$a^2G_{7/2}$-$z^2G_{7/2}$	4.3
-103	3901.656	TiII	(34)	$a^2G_{9/2}$-$z^2G_{9/2}$	4.3
-99	5130.581	TiII	(86)	$b^2G_{9/2}$-$z^2G_{9/2}$	4.3
-118	3566.986	TiII	(40)	$a^4P_{3/2}$-$z^2S_{1/2}$	4.6
-95	3625.858	TiII	(52)	$a^2P_{1/2}$-$z^2S_{1/2}$	4.6
-100	3642.369	TiII	(52)	$a^2P_{3/2}$-$z^2S_{1/2}$	4.6
-114	4781.321	TiII	(92)	$b^2P_{1/2}$-$z^2S_{1/2}$	4.6
-101	4806.428	TiII	(92)	$b^2P_{3/2}$-$z^2S_{1/2}$	4.6
-97	3237.052	TiII	(23)	$a^2D_{3/2}$-$y^2D_{3/2}$	4.9
-144	3240.598	TiII	(23)	$a^2D_{5/2}$-$y^2D_{3/2}$	4.9
-100	3253.879	TiII	(23)	$a^2D_{5/2}$-$y^2D_{5/2}$	4.9
-98	3229.534	TiII	(24)	$a^2D_{3/2}$-$z^2P_{1/2}$	4.9
-157	3279.868	TiII	(24)	$a^2D_{5/2}$-$z^2P_{3/2}$	4.9
-82	3403.400	TiII	(54)	$a^2P_{1/2}$-$z^2P_{3/2}$	4.9
-124	3384.541	TiII	(63)	$b^4P_{3/2}$-$y^2D_{5/2}$	4.9
-98	3707.271	TiII	(72)	$b^2D_{3/2}$-$y^2D_{3/2}$	4.9
-95	3742.699	TiII	(72)	$b^2D_{5/2}$-$y^2D_{5/2}$	4.9

Table 3. continued.

Velocity (km/s)	λ_{lab} (Å)	Ion	Mult.	Transition	E_{exc} (eV)
-79	3758.756	TiII	(73)	$b^2D_{3/2}$-$z^2P_{3/2}$	4.9
-88	3777.124	TiII	(73)	$b^2D_{5/2}$-$z^2P_{3/2}$	4.9
-80	4331.463	TiII	(93)	$b^2P_{1/2}$-$y^2D_{3/2}$	4.9
-100	5212.987	TiII	(103)	$b^2F_{7/2}$-$y^2F_{7/2}$	5.0
-105	3203.463	TiII	(26)	$a^2D_{3/2}$-$y^2F_{5/2}$	5.0
-114	3191.802	TiII	(26)	$a^2D_{5/2}$-$y^2F_{7/2}$	5.0
-107	3217.833	TiII	(36)	$a^2G_{7/2}$-$y^2F_{7/2}$	5.0
-175	3230.364	TiII	(36)	$a^2G_{9/2}$-$y^2F_{7/2}$	5.0
-129	3277.716	TiII	(45)	$a^4P_{5/2}$-$z^4S_{3/2}$	5.0
-102	3316.268	TiII	(65)	$b^4P_{1/2}$-$z^4S_{3/2}$	5.0
-99	3322.655	TiII	(65)	$b^4P_{3/2}$-$z^4S_{3/2}$	5.0
-105	3333.069	TiII	(65)	$b^4P_{5/2}$-$z^4S_{3/2}$	5.0
-111	3283.271	TiII	(66)	$b^4P_{1/2}$-$y^4D_{1/2}$	5.0
-137	3273.016	TiII	(66)	$b^4P_{1/2}$-$y^4D_{3/2}$	5.0
-165	3289.531	TiII	(66)	$b^4P_{3/2}$-$y^4D_{1/2}$	5.0
-99	3279.237	TiII	(66)	$b^4P_{3/2}$-$y^4D_{3/2}$	5.0
-107	3262.557	TiII	(66)	$b^4P_{3/2}$-$y^4D_{5/2}$	5.0
-99	3272.598	TiII	(66)	$b^4P_{5/2}$-$y^4D_{5/2}$	5.0
-100	3663.281	TiII	(75)	$b^2D_{3/2}$-$y^2F_{5/2}$	5.0
-92	3660.804	TiII	(75)	$b^2D_{5/2}$-$y^2F_{7/2}$	5.0
-98	4054.979	TiII	(87)	$b^2G_{7/2}$-$y^2F_{5/2}$	5.0
-100	4029.481	TiII	(87)	$b^2G_{9/2}$-$y^2F_{7/2}$	5.0
-97	2833.015	TiII	(uv7)	$a^2F_{5/2}$-$y^2F_{5/2}$	5.0
-104	3156.562	TiII	(37)	$a^2G_{9/2}$-$y^4D_{7/2}$	5.1
-104	3249.542	TiII	(66)	$b^4P_{5/2}$-$y^4D_{7/2}$	5.1
-12	3057.646	TiII	(47)	$a^4P_{1/2}$-$z^4P_{3/2}$	5.2
-103	3067.404	TiII	(47)	$a^4P_{3/2}$-$z^4P_{1/2}$	5.2
-29	3047.583	TiII	(47)	$a^4P_{3/2}$-$z^4P_{5/2}$	5.2
-38	3072.153	TiII	(47)	$a^4P_{5/2}$-$z^4P_{3/2}$	5.2
-144	3058.990	TiII	(47)	$a^4P_{5/2}$-$z^4P_{5/2}$	5.2
-89	3105.996	TiII	(67)	$b^4P_{1/2}$-$z^4P_{3/2}$	5.2
-105	3111.597	TiII	(67)	$b^4P_{3/2}$-$z^4P_{3/2}$	5.2
-98	3098.095	TiII	(67)	$b^4P_{3/2}$-$z^4P_{5/2}$	5.2
-62	3120.730	TiII	(67)	$b^4P_{5/2}$-$z^4P_{3/2}$	5.2
-90	3107.147	TiII	(67)	$b^4P_{5/2}$-$z^4P_{5/2}$	5.2
-102	4368.886	TiII	(104)	$b^2F_{7/2}$-$y^2G_{9/2}$	5.4
-102	3225.172	TiII	(84)	$a^2H_{11/2}$-$y^2G_{9/2}$	5.4
-95	4550.892	TiII	(84)	$a^2H_{11/2}$-$y^2G_{9/2}$	5.4
-94	3219.193	TiII	(84)	$a^2H_{9/2}$-$y^2G_{7/2}$	5.4
-102	4573.249	TiII	(84)	$a^2H_{9/2}$-$y^2G_{7/2}$	5.4
-98	3511.849	TiII	(88)	$b^2G_{7/2}$-$y^2G_{7/2}$	5.4
-109	3505.899	TiII	(88)	$b^2G_{9/2}$-$y^2G_{9/2}$	5.4
-85	2878.282	TiII	(uv14)	$a^2G_{7/2}$-$y^2G_{7/2}$	5.4
-96	2884.960	TiII	(uv14)	$a^2G_{9/2}$-$y^2G_{9/2}$	5.4
-101	4173.086	TiII	(105)	$b^2F_{5/2}$-$x^2D_{3/2}$	5.6
-99	4164.822	TiII	(105)	$b^2F_{7/2}$-$x^2D_{5/2}$	5.6
-100	3521.271	TiII	(98)	$b^2P_{1/2}$-$x^2D_{3/2}$	5.6
-98	3536.420	TiII	(98)	$b^2P_{3/2}$-$x^2D_{5/2}$	5.6
-78	3453.467	TiII	(99)	$b^2P_{1/2}$-$y^2P_{1/2}$	5.6
-94	3457.378	TiII	(99)	$b^2P_{3/2}$-$y^2P_{3/2}$	5.6
-114	2714.564	TiII	(uv13)	$a^2D_{3/2}$-$y^2P_{3/2}$	5.6
-104	2817.191	TiII	(uv17)	$a^2P_{3/2}$-$y^2P_{1/2}$	5.6
-96	2811.134	TiII	(uv17)	$a^2P_{3/2}$-$y^2P_{3/2}$	5.6

Table 3. continued.

Velocity (km/s)	λ_{lab} (Å)	Ion	Mult.	Transition	E_{exc} (eV)
-116	3018.063	TiII	(85)	$a^2H_{11/2}$-$z^2H_{11/2}$	5.7
-100	3009.188	TiII	(85)	$a^2H_{9/2}$-$z^2H_{11/2}$	5.7
-94	3030.611	TiII	(85)	$a^2H_{9/2}$-$z^2H_{9/2}$	5.7
-81	3288.608	TiII	(89)	$b^2G_{7/2}$-$z^2H_{9/2}$	5.7
-105	3262.525	TiII	(89)	$b^2G_{9/2}$-$z^2H_{11/2}$	5.7
-101	3090.306	TiII	(90)	$b^2G_{7/2}$-$x^2F_{5/2}$	5.9
-94	3104.712	TiII	(90)	$b^2G_{9/2}$-$x^2F_{7/2}$	5.9
-90	10128.770	[TiII]	(5F)	$a^4F_{3/2}$-$b^4P_{1/2}$	1.2
-103	10069.850	[TiII]	(5F)	$a^4F_{3/2}$-$b^4P_{3/2}$	1.2
-100	10069.740	[TiII]	(5F)	$a^4F_{5/2}$-$b^4P_{5/2}$	1.2
-95	8531.906	[TiII]	(15F)	$b^4F_{3/2}$-$b^2D_{3/2}$	1.6
-103	8587.494	[TiII]	(15F)	$b^4F_{5/2}$-$b^2D_{3/2}$	1.6
-116	8664.452	[TiII]	(15F)	$b^4F_{7/2}$-$b^2D_{3/2}$	1.6
-104	8568.400	[TiII]	(15F)	$b^4F_{7/2}$-$b^2D_{5/2}$	1.6
-94	8663.807	[TiII]	(15F)	$b^4F_{9/2}$-$b^2D_{5/2}$	1.6
-119	7918.452	[TiII]	(6F)	$a^4F_{3/2}$-$b^2D_{3/2}$	1.6
-56	7977.897	[TiII]	(6F)	$a^4F_{5/2}$-$b^2D_{3/2}$	1.6
-110	7979.330	[TiII]	(6F)	$a^4F_{7/2}$-$b^2D_{5/2}$	1.6
-107	9408.356	[TiII]	(21F)	$a^2F_{5/2}$-$b^2G_{9/2}$	1.9
-90	9645.089	[TiII]	(21F)	$a^2F_{7/2}$-$b^2G_{7/2}$	1.9
-92	9652.716	[TiII]	(21F)	$a^2F_{7/2}$-$b^2G_{9/2}$	1.9
-88	6648.980	[TiII]	(8F)	$a^4F_{7/2}$-$b^2G_{7/2}$	1.9
-105	6652.610	[TiII]	(8F)	$a^4F_{7/2}$-$b^2G_{9/2}$	1.9
-97	6727.670	[TiII]	(8F)	$a^4F_{9/2}$-$b^2G_{9/2}$	1.9
-98	8412.354	[TiII]	(–)	$a^2F_{5/2}$-$b^2P_{1/2}$	2.0
-100	8335.590	[TiII]	(–)	$a^2F_{5/2}$-$b^2P_{3/2}$	2.1
-99	8526.997	[TiII]	(–)	$a^2F_{5/2}$-$b^2P_{3/2}$	2.1
-95	6126.311	[TiII]	(22F)	$a^2F_{5/2}$-$b^2F_{5/2}$	2.6
-83	6148.896	[TiII]	(22F)	$a^2F_{5/2}$-$b^2F_{7/2}$	2.6
-91	6228.990	[TiII]	(22F)	$a^2F_{7/2}$-$b^2F_{5/2}$	2.6
-95	6252.341	[TiII]	(22F)	$a^2F_{7/2}$-$b^2F_{7/2}$	2.6
-96	4918.247	[TiII]	(23F)	$a^2F_{5/2}$-$c^2D_{3/2}$	3.1
-106	4984.205	[TiII]	(23F)	$a^2F_{7/2}$-$c^2D_{3/2}$	3.1
-101	4927.288	[TiII]	(23F)	$a^2F_{7/2}$-$c^2D_{5/2}$	3.1
-91	6153.623	[TiII]	(26F)	$a^2D_{3/2}$-$c^2D_{3/2}$	3.1
-87	6079.567	[TiII]	(26F)	$a^2D_{5/2}$-$c^2D_{5/2}$	3.1
-119	3126.182	VII	(1)	a^5F_1-z^5G_2	4.3
-101	3134.235	VII	(1)	a^5F_2-z^5G_2	4.3
-117	3119.277	VII	(1)	a^5F_2-z^5G_3	4.3
-96	3146.237	VII	(1)	a^5F_3-z^5G_2	4.3
-93	3131.164	VII	(1)	a^5F_3-z^5G_3	4.3
-105	3111.597	VII	(1)	a^5F_3-z^5G_4	4.3
-209	3127.117	VII	(1)	a^5F_4-z^5G_4	4.3
-98	3146.262	VII	(1)	a^5F_5-z^5G_4	4.3
-107	3103.189	VII	(1)	a^5F_4-z^5G_5	4.4
-187	3122.041	VII	(1)	a^5F_5-z^5G_5	4.4
-109	3094.003	VII	(1)	a^5F_5-z^5G_6	4.4
-98	2935.249	VII	(2)	a^5F_1-z^5F_2	4.5
-96	2942.347	VII	(2)	a^5F_2-z^5F_2	4.5
-84	2952.922	VII	(2)	a^5F_3-z^5F_2	4.5
-95	3593.050	VII	(4)	a^3F_3-z^5F_2	4.5
-85	3590.773	VII	(5)	a^3F_2-z^3D_1	4.5
-91	2958.374	VII	(uv11)	a^5F_2-z^3D_1	4.5

Table 3. continued.

Velocity (km/s)	λ_{lab} (Å)	Ion	Mult.	Transition	E_{exc} (eV)
-102	3917.519	VII	(10)	a^3P_1-z^3D_2	4.6
-94	3953.083	VII	(10)	a^3P_2-z^3D_3	4.6
-95	2918.207	VII	(2)	a^5F_2-z^5F_1	4.6
-104	2921.226	VII	(2)	a^5F_2-z^5F_3	4.6
-107	2931.649	VII	(2)	a^5F_3-z^5F_3	4.6
-94	2945.422	VII	(2)	a^5F_4-z^5F_3	4.6
-95	2924.862	VII	(2)	a^5F_5-z^5F_5	4.6
-100	3531.769	VII	(4)	a^3F_2-z^5F_1	4.6
-92	3594.355	VII	(4)	a^3F_4-z^5F_3	4.6
-95	3546.206	VII	(5)	a^3F_3-z^3D_2	4.6
-106	3525.719	VII	(5)	a^3F_3-z^3D_3	4.6
-97	3557.811	VII	(5)	a^3F_4-z^3D_3	4.6
-108	3897.259	VII	(9)	a^3P_0-z^5F_1	4.6
-95	3998.250	VII	(9)	a^3P_2-z^5F_3	4.6
-92	2716.463	VII	(uv1)	a^5D_2-z^5F_3	4.6
-102	2716.557	VII	(uv1)	a^5D_4-z^5F_4	4.6
-103	2701.736	VII	(uv1)	a^5D_4-z^5F_5	4.6
-86	2908.310	VII	(uv10)	a^5F_4-z^5F_5	4.6
-97	2903.913	VII	(uv11)	a^5F_1-z^3D_2	4.6
-90	2897.040	VII	(uv11)	a^5F_2-z^3D_3	4.6
-102	2921.209	VII	(uv11)	a^5F_3-z^3D_2	4.6
-99	2907.290	VII	(uv11)	a^5F_3-z^3D_3	4.6
-95	2890.463	VII	(uv12)	a^5F_1-z^5D_0	4.6
-108	2892.483	VII	(uv12)	a^5F_2-z^5D_1	4.6
-88	2883.339	VII	(uv12)	a^5F_2-z^5D_2	4.6
-96	2893.493	VII	(uv12)	a^5F_2-z^5D_2	4.6
-111	2702.989	VII	(uv2)	a^5D_3-z^3D_3	4.6
-112	2712.544	VII	(uv2)	a^5D_4-z^3D_3	4.6
-113	2683.887	VII	(uv3)	a^5D_0-z^5D_1	4.6
-82	2691.590	VII	(uv3)	a^5D_2-z^5D_1	4.6
-88	2683.671	VII	(uv3)	a^5D_2-z^5D_2	4.6
-104	2688.760	VII	(uv3)	a^5D_4-z^5D_4	4.6
-102	3904.374	VII	(11)	a^3P_2-z^5D_3	4.7
-100	3518.307	VII	(6)	a^3F_4-z^5D_3	4.7
-97	2880.861	VII	(uv12)	a^5F_3-z^5D_3	4.7
-97	2894.159	VII	(uv12)	a^5F_4-z^5D_3	4.7
-74	2893.279	VII	(uv12)	a^5F_4-z^5D_4	4.7
-98	2909.660	VII	(uv12)	a^5F_5-z^5D_4	4.7
-94	2679.371	VII	(uv3)	a^5D_3-z^5D_4	4.7
-88	2689.519	VII	(uv3)	a^5D_4-z^5D_3	4.7
-102	3746.875	VII	(15)	a^3H_4-z^3G_3	4.9
-88	3733.824	VII	(15)	a^3H_5-z^3G_4	4.9
-96	3716.545	VII	(15)	a^3H_6-z^3G_5	4.9
-91	4036.767	VII	(32)	a^3G_3-z^3G_3	4.9
-97	4024.525	VII	(32)	a^3G_4-z^3G_4	4.9
-105	4006.838	VII	(32)	a^3G_5-z^3G_5	4.9
-108	3268.632	VII	(7)	a^3F_2-z^3G_3	4.9
-99	3299.684	VII	(7)	a^3F_4-z^3G_4	4.9
-69	3277.061	VII	(7)	a^3F_4-z^3G_5	4.9
-94	3772.046	VII	(21)	b^3F_2-z^3F_2	5.0
-77	3751.944	VII	(21)	b^3F_3-z^3F_3	5.0
-88	3188.624	VII	(8)	a^3F_2-z^3F_2	5.0
-95	3191.602	VII	(8)	a^3F_4-z^3F_4	5.0

Table 3. continued.

Velocity (km/s)	λ_{lab} (Å)	Ion	Mult.	Transition	E_{exc} (eV)
-91	2996.863	VII	(27)	a^5P_1-z^5P_2	5.8
-90	3015.694	VII	(27)	a^5P_2-z^5P_1	5.8
-90	3002.079	VII	(27)	a^5P_3-z^5P_3	5.8
-91	3013.985	VII	(28)	a^5P_1-y^5D_1	5.8
-81	3021.542	VII	(28)	a^5P_2-y^5D_1	5.8
-79	2969.241	VII	(28)	a^5P_3-y^5D_4	5.9
-90	3054.279	VII	(34)	a^3G_4-z^3H_5	5.9
-129	3034.702	VII	(34)	a^3G_5-z^3H_6	5.9
-87	3101.834	VII	(39)	b^3G_3-y^3G_3	6.0
-115	3094.056	VII	(39)	b^3G_5-y^3G_5	6.1
-90	3234.705	VII	(61)	a^3D_3-y^3F_4	6.1
-98	2766.497	VII	(uv46)	a^3H_6-y^3G_5	6.1
-100	3137.439	VII	(122)	b^3H_5-y^3H_5	6.5
-91	3034.318	VII	(123)	b^3H_6-z^3I_7	6.6
-111	2818.332	VII	(120)	a^3D_1-w^3D_1	6.7
-39	2932.480	VII	(–)	b^3D_2-x^3P_1	6.8
-110	2933.179	VII	(–)	b^3D_3-x^3P_2	6.8
-94	8881.373	[VII]	(2F)	a^5D_1-a^3P_0	1.4
-97	8765.679	[VII]	(2F)	a^5D_2-a^3P_1	1.4
-110	8473.399	[VII]	(2F)	a^5D_2-a^3P_2	1.5
-95	7499.749	[VII]	(3F)	a^5D_3-b^3F_3	1.7
-162	7462.648	[VII]	(3F)	a^5D_3-b^3F_4	1.7
-96	7535.937	[VII]	(3F)	a^5D_4-b^3F_4	1.7
-74	7355.792	[VII]	(4F)	a^5D_0-a^5P_2	1.7
-89	7334.077	[VII]	(4F)	a^5D_2-a^5P_3	1.7
-94	7517.180	[VII]	(4F)	a^5D_3-a^5P_1	1.7
-94	7544.026	[VII]	(4F)	a^5D_4-a^5P_2	1.7
-110	7461.350	[VII]	(4F)	a^5D_4-a^5P_3	1.7
-87	7346.030	[VII]	(12F)	a^5F_3-b^3G_4	2.0
-94	7479.321	[VII]	(12F)	a^5F_5-b^3G_5	2.0
-121	7549.997	[VII]	(–)	a^5P_2-a^1F_3	3.3
-86	2867.582	CrII	(uv5)	$a^6D_{3/2}$-$z^6F_{3/2}$	5.8
-92	2856.509	CrII	(uv5)	$a^6D_{3/2}$-$z^6F_{5/2}$	5.8
-86	2865.943	CrII	(uv5)	$a^6D_{5/2}$-$z^6F_{5/2}$	5.8
-102	2850.675	CrII	(uv5)	$a^6D_{5/2}$-$z^6F_{7/2}$	5.9
-102	2863.412	CrII	(uv5)	$a^6D_{7/2}$-$z^6F_{7/2}$	5.9
-88	2844.085	CrII	(uv5)	$a^6D_{7/2}$-$z^6F_{9/2}$	5.9
-91	2836.463	CrII	(uv5)	$a^6D_{9/2}$-$z^6F_{11/2}$	5.9
-101	2859.749	CrII	(uv5)	$a^6D_{9/2}$-$z^6F_{9/2}$	5.9
16	3422.183	CrII	(3)	$a^4D_{1/2}$-$z^4P_{1/2}$	6.0
-119	3423.714	CrII	(3)	$a^4D_{5/2}$-$z^4P_{3/2}$	6.1
94	3359.456	CrII	(4)	$a^4D_{5/2}$-$z^6D_{3/2}$	6.1
-212	3409.735	CrII	(4)	$a^4D_{7/2}$-$z^6D_{5/2}$	6.1
-118	2664.467	CrII	(uv8)	$a^6D_{1/2}$-$z^6D_{1/2}$	6.1
-118	2679.585	CrII	(uv8)	$a^6D_{3/2}$-$z^6D_{5/2}$	6.1
-113	2687.885	CrII	(uv8)	$a^6D_{5/2}$-$z^6D_{5/2}$	6.1
-99	2666.813	CrII	(uv8)	$a^6D_{5/2}$-$z^6D_{7/2}$	6.1
-83	2699.210	CrII	(uv8)	$a^6D_{7/2}$-$z^6D_{5/2}$	6.1
-110	2691.839	CrII	(uv8)	$a^6D_{9/2}$-$z^6D_{7/2}$	6.1
-125	3369.009	CrII	(3)	$a^4D_{7/2}$-$z^4P_{5/2}$	6.2
-112	2673.621	CrII	(uv7)	$a^6D_{7/2}$-$z^4P_{5/2}$	6.2
-89	2664.214	CrII	(uv8)	$a^6D_{7/2}$-$z^6D_{9/2}$	6.2
-99	2677.955	CrII	(uv8)	$a^6D_{9/2}$-$z^6D_{9/2}$	6.2

Table 3. continued.

Velocity (km/s)	λ_{lab} (Å)	Ion	Mult.	Transition	E_{exc} (eV)
-99	2677.957	CrII	(uv8)	$a^6D_{9/2}$-$z^6D_{9/2}$	6.2
-113	3121.264	CrII	(5)	$a^4D_{3/2}$-$z^4F_{5/2}$	6.4
-90	3125.879	CrII	(5)	$a^4D_{5/2}$-$z^4F_{7/2}$	6.4
-99	3132.961	CrII	(5)	$a^4D_{7/2}$-$z^4F_{9/2}$	6.4
-117	8359.939	[CrII]	(1F)	$a^6S_{5/2}$-$a^6D_{1/2}$	1.5
-129	8310.770	[CrII]	(1F)	$a^6S_{5/2}$-$a^6D_{3/2}$	1.5
-121	8231.930	[CrII]	(1F)	$a^6S_{5/2}$-$a^6D_{5/2}$	1.5
-127	8127.531	[CrII]	(1F)	$a^6S_{5/2}$-$a^6D_{7/2}$	1.5
-115	8002.279	[CrII]	(1F)	$a^6S_{5/2}$-$a^6D_{9/2}$	1.5
-101	4582.145	[CrII]	(3F)	$a^6S_{5/2}$-$a^4P_{1/2}$	2.7
-119	4582.422	[CrII]	(3F)	$a^6S_{5/2}$-$a^4P_{1/2}$	2.7
-97	4582.088	[CrII]	(3F)	$a^6S_{5/2}$-$a^4P_{3/2}$	2.7
-86	3994.340	[CrII]	(4F)	$a^6S_{5/2}$-$b^4D_{1/2}$	3.1
-99	3992.530	[CrII]	(4F)	$a^6S_{5/2}$-$b^4D_{5/2}$	3.1
-107	3994.620	[CrII]	(4F)	$a^6S_{5/2}$-$b^4D_{7/2}$	3.1
-47	3496.833	MnII	(3)	a^5D_0-z^5P_1	5.4
-116	3489.675	MnII	(3)	a^5D_1-z^5P_1	5.4
-117	3475.124	MnII	(3)	a^5D_2-z^5P_1	5.4
-118	3483.902	MnII	(3)	a^5D_2-z^5P_2	5.4
-115	3461.307	MnII	(3)	a^5D_3-z^5P_2	5.4
-110	3475.035	MnII	(3)	a^5D_3-z^5P_3	5.4
-130	3497.810	MnII	(3)	a^5D_3-z^5P_3	5.4
-116	3442.974	MnII	(3)	a^5D_4-z^5P_3	5.4
-185	2933.913	MnII	(uv5)	a^5S_2-z^5P_1	5.4
-119	2940.168	MnII	(uv5)	a^5S_2-z^5P_2	5.4
-115	2950.067	MnII	(uv5)	a^5S_2-z^5P_3	5.4
-126	6852.215	[MnII]	(2F)	a^7S_3-a^5D_3	1.8
-114	6980.380	[MnII]	(2F)	a^7S_3-a^5D_4	1.8
-105	7881.401	[MnII]	(7F)	a^5D_1-a^5G_2	3.4
-92	7807.566	[MnII]	(7F)	a^5D_2-a^5G_2	3.4
-111	7808.041	[MnII]	(7F)	a^5D_2-a^5G_3	3.4
-115	7811.048	[MnII]	(7F)	a^5D_2-a^5G_4	3.4
-117	7705.686	[MnII]	(7F)	a^5D_3-a^5G_5	3.4
-113	7549.797	[MnII]	(7F)	a^5D_4-a^5G_5	3.4
-119	7563.501	[MnII]	(7F)	a^5D_4-a^5G_6	3.4
-99	6658.570	[MnII]	(8F)	a^5D_1-a^5P_2	3.7
-106	6511.434	[MnII]	(8F)	a^5D_3-a^5P_1	3.7
-103	6537.786	[MnII]	(8F)	a^5D_3-a^5P_3	3.7
-105	6412.900	[MnII]	(8F)	a^5D_4-a^5P_2	3.7
-106	6425.224	[MnII]	(8F)	a^5D_4-a^5P_3	3.7
-104	5474.872	[MnII]	(9F)	a^5D_3-b^5D_2	4.1
-135	5475.440	[MnII]	(9F)	a^5D_3-b^5D_3	4.1
-105	5496.302	[MnII]	(9F)	a^5D_3-b^5D_4	4.1
-90	5395.713	[MnII]	(9F)	a^5D_4-b^5D_2	4.1
-121	5396.266	[MnII]	(9F)	a^5D_4-b^5D_3	4.1
-121	5416.528	[MnII]	(9F)	a^5D_4-b^5D_4	4.1
-101	5329.520	FeI	(15)	a^5F_4-z^5D_3	3.2
-78	3887.383	FeI	(4)	a^5D_3-z^5D_3	3.2
-106	3825.529	FeI	(4)	a^5D_4-z^5D_3	3.2
-98	3861.005	FeI	(4)	a^5D_4-z^5D_4	3.2
-95	5372.983	FeI	(15)	a^5F_3-z^5D_2	3.3
-98	3879.672	FeI	(4)	a^5D_2-z^5D_1	3.3
-91	3720.993	FeI	(5)	a^5D_4-z^5F_5	3.3

Table 3. continued.

Velocity (km/s)	λ_{lab} (Å)	Ion	Mult.	Transition	E_{exc} (eV)
-105	3749.327	FeI	(5)	a^5D_1-z^5F_2	3.4
-81	3746.626	FeI	(5)	a^5D_2-z^5F_3	3.4
-87	3684.104	FeI	(5)	a^5D_3-z^5F_2	3.4
-100	3738.194	FeI	(5)	a^5D_3-z^5F_4	3.4
-101	3680.961	FeI	(5)	a^5D_4-z^5F_4	3.4
-107	3441.592	FeI	(6)	a^5D_4-z^5P_3	3.6
-105	3466.853	FeI	(6)	a^5D_1-z^5P_1	3.7
-99	3821.509	FeI	(20)	a^5F_5-y^5D_4	4.1
-97	3059.975	FeI	(9)	a^5D_3-y^5D_4	4.1
-79	3021.519	FeI	(9)	a^5D_4-y^5D_4	4.1
-102	2967.764	FeI	(10)	a^5D_4-y^5F_5	4.2
-96	3851.061	FeI	(20)	a^5F_1-y^5D_0	4.2
-94	3866.619	FeI	(20)	a^5F_1-y^5D_1	4.2
-79	3841.526	FeI	(20)	a^5F_2-y^5D_1	4.2
-94	3873.599	FeI	(20)	a^5F_2-y^5D_2	4.2
-95	3835.310	FeI	(20)	a^5F_3-y^5D_2	4.2
-95	3826.966	FeI	(20)	a^5F_4-y^5D_3	4.2
-89	3750.551	FeI	(21)	a^5F_4-y^5F_4	4.2
-96	3735.926	FeI	(21)	a^5F_5-y^5F_5	4.2
-99	3026.724	FeI	(9)	a^5D_0-y^5D_1	4.2
-83	3009.017	FeI	(9)	a^5D_1-y^5D_0	4.2
-102	3038.273	FeI	(9)	a^5D_1-y^5D_2	4.2
-118	3048.491	FeI	(9)	a^5D_2-y^5D_3	4.2
-89	2995.300	FeI	(9)	a^5D_3-y^5D_2	4.2
-122	3021.953	FeI	(9)	a^5D_3-y^5D_3	4.2
-93	3768.262	FeI	(21)	a^5F_1-y^5F_1	4.3
-84	3788.956	FeI	(21)	a^5F_1-y^5F_2	4.3
-90	3744.426	FeI	(21)	a^5F_2-y^5F_1	4.3
-95	3764.858	FeI	(21)	a^5F_2-y^5F_2	4.3
-100	3796.080	FeI	(21)	a^5F_2-y^5F_3	4.3
-106	3728.679	FeI	(21)	a^5F_3-y^5F_2	4.3
-122	3759.301	FeI	(21)	a^5F_3-y^5F_3	4.3
-50	3710.301	FeI	(21)	a^5F_4-y^5F_3	4.3
-93	3648.881	FeI	(23)	a^5F_4-z^5G_5	4.3
-108	3582.217	FeI	(23)	a^5F_5-z^5G_6	4.3
-99	4384.776	FeI	(41)	a^3F_4-z^5G_5	4.3
-94	3609.888	FeI	(23)	a^5F_1-z^5G_2	4.4
-72	3588.008	FeI	(23)	a^5F_2-z^5G_2	4.4
-90	3619.800	FeI	(23)	a^5F_2-z^5G_3	4.4
-114	3586.342	FeI	(23)	a^5F_3-z^5G_3	4.4
-147	3632.498	FeI	(23)	a^5F_3-z^5G_4	4.4
-69	3566.397	FeI	(24)	a^5F_3-z^3G_4	4.4
-95	3571.116	FeI	(24)	a^5F_4-z^3G_5	4.4
-82	4416.362	FeI	(41)	a^3F_2-z^5G_3	4.4
-91	4405.987	FeI	(41)	a^3F_3-z^5G_4	4.4
-106	4295.332	FeI	(41)	a^3F_4-z^5G_4	4.4
-105	4309.114	FeI	(42)	a^3F_3-z^3G_4	4.4
-99	4203.212	FeI	(42)	a^3F_4-z^3G_4	4.4
-99	4272.961	FeI	(42)	a^3F_4-z^3G_5	4.4
-95	4145.038	FeI	(43)	a^3F_3-y^3F_4	4.5
-97	4046.956	FeI	(43)	a^3F_4-y^3F_4	4.5
-101	4064.742	FeI	(43)	a^3F_3-y^3F_3	4.6
-95	2721.709	FeI	(uv5)	a^5D_3-y^5P_2	4.6

Table 3. continued.

Velocity (km/s)	λ_{lab} (Å)	Ion	Mult.	Transition	E_{exc} (eV)
-87	2719.833	FeI	(uv5)	a^5D_4-y^5P_3	4.6
-110	4072.887	FeI	(43)	a^3F_2-y^3F_2	4.7
-70	4006.373	FeI	(43)	a^3F_3-y^3F_2	4.7
-99	3816.923	FeI	(45)	a^3F_4-y^3D_3	4.7
-94	3828.909	FeI	(45)	a^3F_3-y^3D_2	4.8
-80	3058.335	FeI	(28)	a^5F_5-x^5D_4	4.9
-61	3101.565	FeI	(28)	a^5F_3-x^5D_3	5.0
-86	3042.623	FeI	(30)	a^5F_3-x^5F_4	5.0
-90	3010.446	FeI	(30)	a^5F_4-x^5F_4	5.0
-90	3000.387	FeI	(30)	a^5F_5-x^5F_5	5.0
-93	4483.510	FeI	(68)	a^5P_1-x^5D_2	5.0
-101	2541.735	FeI	(uv7)	a^5D_1-x^5D_2	5.0
-105	2511.591	FeI	(uv7)	a^5D_3-x^5D_2	5.0
-176	3043.549	FeI	(30)	a^5F_2-x^5F_3	5.1
-78	3019.862	FeI	(30)	a^5F_3-x^5F_3	5.1
-95	2490.501	FeI	(uv9)	a^5D_0-x^5F_1	5.1
-103	2491.907	FeI	(uv9)	a^5D_1-x^5F_2	5.1
-95	2491.395	FeI	(uv9)	a^5D_2-x^5F_3	5.1
-77	2814.116	FeI	(uv44)	a^5F_4-y^5G_5	5.3
-95	2734.390	FeI	(–)	a^5F_5-w^5D_4	5.4
-132	3775.896	FeI	(73)	a^5P_1-w^5D_1	5.5
-103	2712.459	FeI	(uv47)	a^5F_4-w^5F_5	5.5
-112	2731.790	FeI	(uv48)	a^5F_1-v^5D_1	5.5
-106	2591.646	FeI	(–)	a^5F_3-w^5P_2	5.7
-98	3864.836	FeI	(280)	a^3G_5-w^5G_4	5.9
-91	2493.573	FeI	(uv59)	a^5F_3-w^5G_2	5.9
-103	2493.383	FeI	(uv63)	a^5F_3-x^3G_3	5.9
-109	3234.901	FeI	(158)	z^7D_4-e^7P_4	6.3
-102	4150.535	FeI	(694)	z^5F_5-e^7G_6	6.3
-95	2576.820	FeI	(–)	a^3G_4-sp^3F_3	7.5
-72	3296.766	FeII	(1)	$a^4D_{3/2}$-$z^6D_{3/2}$	4.8
-83	3256.826	FeII	(1)	$a^4D_{7/2}$-$z^6D_{7/2}$	4.8
	2607-2632	FeII	(uv1)	a^6D-z^6D	5.0
-97	2971.382	FeII	(2)	$a^4D_{3/2}$-$z^6F_{5/2}$	5.2
-69	2980.224	FeII	(2)	$a^4D_{1/2}$-$z^6F_{3/2}$	5.3
-120	2750.134	FeII	(uv62)	$a^4D_{5/2}$-$z^4F_{7/2}$	5.5
-110	2756.552	FeII	(uv62)	$a^4D_{7/2}$-$z^4F_{9/2}$	5.5
-112	2740.359	FeII	(uv63)	$a^4D_{7/2}$-$z^4D_{7/2}$	5.5
-97	2744.008	FeII	(uv62)	$a^4D_{1/2}$-$z^4F_{3/2}$	5.6
-121	2747.296	FeII	(uv62)	$a^4D_{1/2}$-$z^4F_{5/2}$	5.6
-138	2750.299	FeII	(uv63)	$a^4D_{1/2}$-$z^4D_{1/2}$	5.6
-100	2762.629	FeII	(uv63)	$a^4D_{1/2}$-$z^4D_{3/2}$	5.6
-94	2737.776	FeII	(uv63)	$a^4D_{3/2}$-$z^4D_{1/2}$	5.6
-83	2728.347	FeII	(uv63)	$a^4D_{5/2}$-$z^4D_{3/2}$	5.6
-96	2715.218	FeII	(uv63)	$a^4D_{7/2}$-$z^4D_{5/2}$	5.6
-116	2567.682	FeII	(uv64)	$a^4D_{3/2}$-$z^4P_{1/2}$	5.9
-86	2578.695	FeII	(uv78)	$a^4P_{1/2}$-$z^4P_{1/2}$	5.9
-101	8349.870	[FeI]	(1F)	a^5D_4-a^3F_4	1.5
-106	5938.647	[FeI]	(2F)	a^5D_1-a^5P_2	2.2
-103	5806.063	[FeI]	(2F)	a^5D_2-a^5P_1	2.2
-104	5936.067	[FeI]	(2F)	a^5D_2-a^5P_3	2.2
-96	5710.551	[FeI]	(2F)	a^5D_3-a^5P_1	2.2
-95	5836.266	[FeI]	(2F)	a^5D_3-a^5P_3	2.2

Table 3. continued.

Velocity (km/s)	λ_{lab} (Å)	Ion	Mult.	Transition	E_{exc} (eV)
-101	5697.949	[FeI]	(2F)	a^5D_4-a^5P_3	2.2
-91	5641.119	[FeI]	(2F)	a^5D_4-a^5P_2	2.3
-105	4844.701	[FeI]	(4F)	a^5D_4-b^3F2_4	2.6
-116	7007.180	[FeI]	(15F)	a^5F_3-a^3G_4	2.7
-90	6838.838	[FeI]	(15F)	a^5F_4-a^3G_4	2.7
-104	6974.000	[FeI]	(15F)	a^5F_4-a^3G_5	2.7
-89	6762.484	[FeI]	(15F)	a^5F_5-a^3G_5	2.7
-39	4623.490	[FeI]	(21F)	a^5F_3-b^3D_2	3.6
-110	9338.400	[CoII]	(1F)	a^3F_4-b^3F_3	1.3
-95	9641.850	[CoII]	(1F)	a^3F_3-b^3F_2	1.4
-103	7276.590	[CoII]	(3F)	a^5F_4-a^5P_3	2.2
-126	6934.270	[CoII]	(3F)	a^5F_5-a^5P_3	2.2
-105	4153.755	[CoII]	(–)	a^3F_4-b^3P_2	3.0
-106	6925.736	[CoII]	(–)	b^3F_3-b^1G_4	3.1
-101	6521.281	[CoII]	(–)	b^3F_4-b^1G_4	3.1
-110	7102.208	[CoII]	(–)	a^3P_1-a^3D_3	3.4
-113	8303.270	[NiII]	(2F)	$a^2D_{3/2}$-$a^2F_{7/2}$	1.7
-112	7379.970	[NiII]	(2F)	$a^2D_{5/2}$-$a^2F_{7/2}$	1.7
-100	7413.690	[NiII]	(2F)	$a^2D_{3/2}$-$a^2F_{5/2}$	1.9
-109	6668.670	[NiII]	(2F)	$a^2D_{5/2}$-$a^2F_{5/2}$	1.9
-181	4327.453	[NiII]	(4F)	$a^2D_{5/2}$-$a^4P_{5/2}$	2.9
-74	7257.860	[NiII]	(8F)	$a^4F_{7/2}$-$a^4P_{5/2}$	2.9
-93	6793.350	[NiII]	(8F)	$a^4F_{5/2}$-$a^4P_{1/2}$	3.1
-66	6815.450	[NiII]	(8F)	$a^4F_{5/2}$-$a^4P_{3/2}$	3.1
-101	4216.706	SrII	(1)	$a^2S_{1/2}$-$a^2P_{1/2}$	2.9
-101	4078.860	SrII	(1)	$a^2S_{1/2}$-$a^2P_{3/2}$	3.0
-88	6870.070	[SrII]	(1F)	$a^2S_{1/2}$-$a^2D_{3/2}$	1.8
-89	6740.230	[SrII]	(1F)	$a^2S_{1/2}$-$a^2D_{5/2}$	1.8

Table 4. Unidentified lines

λ_{obs} (Å)	Int (nov01)[a]	Wavelength coincidence
2537.92	14	bl
2538.90	22	
2548.76	7	VII a^3P_1-y^3P_1
2580.24	37	
2592.96	33	bl abs
2815.20	3[b]	FeI a^3F_2-sp^5H_3
3050.49	8	VII a^3D_3-y^3P_2
3146.64	5	
3208.63	8	
3379.87	19	TiII $b^4P_{5/2}$-$y^2D_{3/2}$
3391.76	15	ZrII $a^4F_{9/2}$-$z^4G_{11/2}$
3414.65	7	VII b^3D_3-z^1D_2
3416.15	13	
3438.51	34	ZrII $a^4F_{7/2}$-$z^4G_{9/2}$, bl.
3600.62	5	YII a^3D_3-z^3D_3
3687.65	11	
3697.79	4	
3709.35	9	YII a^3D_3-z^3F_3, bl.
3774.24	9	TiII $a^2F_{5/2}$-$z^4F_{7/2}$
		YII a^3D_2-z^3F_3
		SrII 5d $^2D_{5/2}$-7f ^2F
3856.35	4	
3958.07	1	ZrII $a^2D_{3/2}$-$z^2F_{5/2}$
4305.24	6	SrII 5p $^2P_{3/2}$-6s $^2S_{1/2}$
4427.25	2	TiII $b^4P_{5/2}$-$z^4D_{3/2}$
4747.17	9	SrII 6s $^2S_{1/2}$-7p $^2P_{1/2}$
4763.86	4	TiII $a^2P_{3/2}$-$z^4F_{5/2}$
4802.32	7	
5253.20	1	FeI z^5D_1-e^5D_1
5303.74	3	[FeI] a^5D_2-a^3P_1
5470.63	7	
5559.85	4	
5599.35	1	
6160.44	2	
6219.08	2	FeI a^5P_2-y^5D_2
6998.68	2	
7426.27	7	
7430.71	4	
7664.71	13	YII a^3D-a^3P
7749.18	4	
7808.06	6	
8050.43	3	
8674.12	2	[VII] a^3F_4-b^3D_3
8698.34	2	[VII] a^5F_5-a^3G_5
8806.31	4	
9341.82	4	

[a] 10^{-15} erg cm^{-2} s^{-1} arcsec^{-2}

[b] The 2815 Å line is not covered in the Nov01 observations. The observed intensity is from the Mar00 data.